Final report for project entitled
"Control of resonances and optical properties of plasmonic-patch metamaterials",
under Award No. FA2386-11-1-4707

The stated research goals of the project were:

The proposal for the year 2011-2012 is to fabricate multilayered plasmonic metamaterials and experimentally study their photonic properties when nonlinear amplifying dye molecules are imbedded in the structures. We will particularly focus on three multilayer systems whose plasmonic resonances can be tuned using the spacer layer thickness. This exploitation of the third dimension is rather unique and has not really been widely utilized yet. All these experimental developments will be strongly supported by computations and theory, which is our strong point.

The following issues will be specifically addressed:

1. Fabrication of multi-layer plasmonic patch / film metamaterials.
2. Measurement of the surface plasmon resonance in the metamaterials
3. Imbedding non-linear and amplifying materials (dye-doped organic materials) into the metamaterial structures.
4. Measurement of plasmon resonance and florescence properties in the dye-doped metamaterials with and without the presence of a pump laser.

Achievements in the project:

The main achievements in the project are that

1. We have been able to fabricate single and multi-layered corrugated gratings and patch metamaterials of plasmonic (gold) films using laser interference lithography.
2. The suface plasman dispersion in these plasmonic corrugated gratings have been measured in great detail using a home-built surface plasmon spectrometer.
3. We have been able to imbed non-linear and amplifying layers in the plasmonic corrugated layers by using rhodamine-6G doped poly methyl methacrylate (PMMA) layers.
4. The fluorescence properties of the dye from the corrugated grating has been studied. The fluorescence can be highly enhanced and this turns out to be primarily due to plasmonic effects in the excitation mechanisms.
5. Studies on surface enhanced Raman scattering from these films were continued and the enhanced SERS was found to be highly correlated with the possibility of finding propagating surface plasmon dispersion branches in the frequency and angle of incidence of the pump laser.
6. Preliminary studies on the surface plasmon dispersion with and without laser amplification in the plasmonic structures have been carried out.

Much of these results have been written up for publication in the following papers (copies attached with the report).

i. P. Mandal, A. Nandi, S. A. Ramakrishna, "*Propagating surface plasmon resonances in patterned gold-grating templates and surface enhanced Raman scattering*", Journal of Applied Physics (AIP) (In Press, 2012)

ii. P. Mandal, Prince Gupta, A. Nandi, and S. Anantha Ramakrishna "*Surface enhanced fluorescence due to localized plasmonic near-field excitation in corrugated gold gratings*", Journal of Nanophotonics (SPIE) (Submitted, 2012)

Report Documentation Page

Form Approved
OMB No. 0704-0188

1. REPORT DATE	2. REPORT TYPE	3. DATES COVERED
01 AUG 2012	**Final**	**04-05-2011 to 03-05-2012**

4. TITLE AND SUBTITLE
Control of resonances and optical properties of plasmonic-patch metamaterials

5a. CONTRACT NUMBER
FA23861114047

5b. GRANT NUMBER

5c. PROGRAM ELEMENT NUMBER

6. AUTHOR(S)
Anantha Ramakrishna

5d. PROJECT NUMBER

5e. TASK NUMBER

5f. WORK UNIT NUMBER

7. PERFORMING ORGANIZATION NAME(S) AND ADDRESS(ES)
Indian Institute of Technology, Kanpur,Office: 487, ,Faculty Building,Kanpur 208 016,NA,NA

8. PERFORMING ORGANIZATION REPORT NUMBER
N/A

9. SPONSORING/MONITORING AGENCY NAME(S) AND ADDRESS(ES)
AOARD, UNIT 45002, APO, AP, 96338-5002

10. SPONSOR/MONITOR'S ACRONYM(S)
AOARD

11. SPONSOR/MONITOR'S REPORT NUMBER(S)
AOARD-114047

12. DISTRIBUTION/AVAILABILITY STATEMENT
Approved for public release; distribution unlimited

13. SUPPLEMENTARY NOTES

14. ABSTRACT
The primary objective of this research is to study the dispersion of the surface plasmon to correlate the physical origins or various phenomena linked to plasmonic effects. The goal is to fabricate multilayered plasmonic metamaterials and experimentally study their photonic properties when nonlinear amplifying dye molecules are imbedded in the structures.

15. SUBJECT TERMS
composite materials, Field Tunable Materials, meta materials, plasmonics

16. SECURITY CLASSIFICATION OF:			17. LIMITATION OF ABSTRACT	18. NUMBER OF PAGES	19a. NAME OF RESPONSIBLE PERSON
a. REPORT	b. ABSTRACT	c. THIS PAGE			
unclassified	**unclassified**	**unclassified**	**Same as Report (SAR)**	**40**	

Below we will present the developments under each of the objectives. Many of the details can be found in the publications referred to above.

Fabrication of large area periodic plasmonic arrays:

We fabricated periodic plasmonic gratings over large areas of about 10 mm diameter, using laser interference lithography (LIL). Essentially, two beams from a blue laser are combined to give rise to an interference pattern, as shown schematically in figure 1. If the angle between the two beams is θ, then the period of the interference pattern is $p = \lambda/2 \sin\theta$. Using a high coherence DPSS laser at 473 nm, gratings with periods ranging from 400 nm to 1300 nm could be fabricated.

Fabrication of plasmonic corrugated gratings was performed by the following steps: Positive-tone photoresist (ma-P1205 from Micro-resist technology, Germany) was spin coated at 3000 rpm for 45 seconds on cleaned glass plates, and subsequently baked at 80°C for 1 minute. The photoresist coated glass plates were then exposed to the two-beam laser interference patterns, typically for 20 minutes. While upto continuous 20 minutes exposure was used to generate one-dimensional (1D) periodic nano-grating templates, the multiple exposure (10 minutes each) method was adapted for the generation of two-dimensional (2D) periodic nano-grating templates. A sample stage rotation of 90° or 60° was performed between the first and the second exposure to generate square or hexagonal patterns, respectively. The development of the exposed photoresist films in a standard developer solution (MPIK) resulted in periodically patterned photoresist films on the glass substrates. A thin layer (40 nm, unless otherwise stated) of gold was thermally evaporated onto the top of the patterns. The thickness of the gold layer was measured in-situ by a piezo-electric sensor and afterwards in some gratings by a contact profilometer to confirm the film thicknesses.

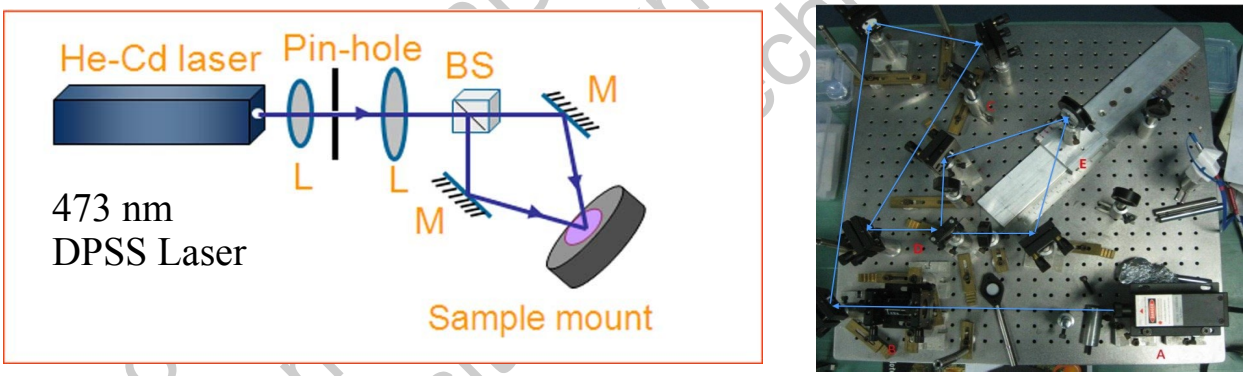

Fig. 1: Schematic diagram of the experimental setup for carrying out laser interference lithography to produce periodic gratings (leftt) and the photograph (right panel) of the compact setup used for the laser interference lithography. The path of the laser beam is traced out as a guide to the eye.

Using the steps above, accurate plasmonic gratings were fabricated. The gratings were characterized by optical microscopy (bright field and dark field) as well as atomic force microscopy. The studies revealed highly ordered periodic structures over almost the entire laser beam area, which was about 10 mm diameter. The atomic force microscopy revealed that the modulation depth in these gratings was about 200 nm. The gratings did not, however, have very edges due to vibrations sustained during the long exposure times necessitated by the low laser power. Hence, technically the gratings would be termed as corrugated gratings with deep corrugations and a continuous gold film, although the gold coatings on the side walls will necessarily be much thinner than on the ridges and valleys due to the physical vapor deposition at normal incidence. Figure 2 shows some images of the corrugated plasmonic gratings obtained with different symmetries as well as the AFM image demonstrating the depth modulation.

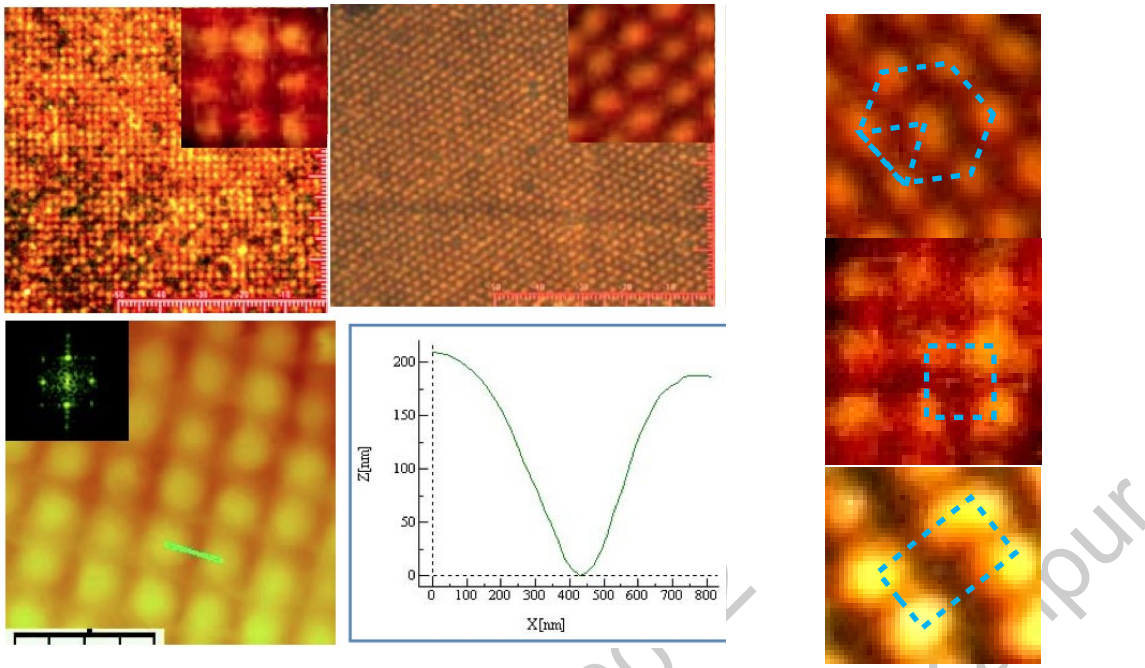

Fig. 2: Top panels: Dark field optical microscope images of the plasmonic gratings with square and hexagonal symmetries. Insets show a magnified view. Bottom panel left shows the atomic force microscopy image of a 800 nm grating with a periodic 2D square lattice, while the bottom right panel shows the depth modulation measured by the atomic force microscope corresponding to the path of the green line shown on the AFM image on the left. The inset in bottom left panel shows the fourier transform of the AFM image demonstrating the long range order. The extreme right panels show the nice symmetrical plasmonic templates obtained by this method and imaged by optical microscopy, (top to bottom): hexagonal, square and rectangular array of pillars, respectively. These structures are grown simply through controlling the exposure parameters such as angle of rotation stage, exposure duration.

Multi-layered plasmonic gratings were fabricated by first creating a corrugated grating using the standard LIL procedure detailed above and then repeatedly applying thin films of gold and PMMA (polymethyl methacrylate) alternatively by thermal evaporation and spin coating at 3000 rpm respectively. The layer thicknesses were chosen to be typically about 20 nm. For these thicknesses, the coatings are almost conformal with the underlying patterned substrate and several coatings can be applied with a slow reduction in the surface modulation with each successive layer. Care has to be taken to keep the grating at a large distance from the vapor source during the thermal evaporation to prevent the underlying films from heating up. In our case, this distance was almost 25 cm. The collimated vapor flux at these distances are also useful to increase the corrugation modulation. Using this method, multilayered corrugated films with 3 to 5 layers were prepared.

Surface plasmon dispersion measurements in plasmonic arrays

One of the primary objectives under this project was to study the dispersion of the surface plasmons . This enables us to correlate the physical origins or various phenomena linked to plasmonic effects. For this, an angle-resolved white light transmission spectrometer was designed and fabricated locally. This was used to monitor the transmission of light as a function of both the angle of incidence and wavelength. When the resonant phase matching conditions for the excitation of surface plasmons are satisfied, the transmission dips in magnitude. Note that in our case, the periodicity couples the free light to surface plasmons through Bragg scattering and no other coupling mechanisms are required. A 2-D plot of the transmissions versus the angle and wavelength enables us to instantly trace out the dispersion of the surface plasmons as shown in Figure 3. The transmission measurements were carried out in the angular range of -40^0 to $+40^0$ with a step of 0.2^0 and a wavelength range of 450 nm to 1000 nm for the gold gratings. The white light source was a

100 watt tungsten-halogen lamp with a final collimated beam width of ~1 mm. A polarizer was used to illuminate the gratings with transverse magnetic (TM) polarization mode of input beam to match sample orientation. Computer programmes to simultaneously control the stepper motor and the Ocean Optics USB2000+ spectrometer were developed in-house to quickly obtain the entire surface plasmon dispersions within few minutes.

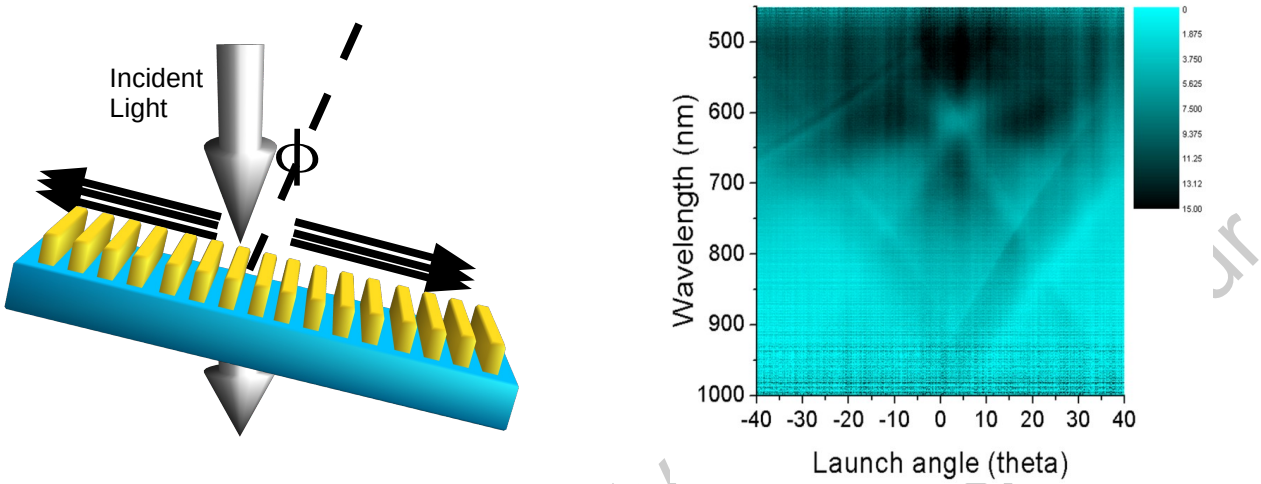

Fig. 3: Left panel – Schematic of the angle dependent transmission of white light through a plasmonic grating. When the coupling angle for surface plasmons is met, the transmission is highly attenuated. Right panel – The transmittance through a corrugated one dimensional gold grating with 600 nm period. The locus of the transmission minima as a function of the wavelength (inverse of frequency) and the angle (parallel wave-vector), allow us to trace out the dispersions of the surface plasmons. Note that the due to Bragg scattering, the surface plasmons get mapped back into the first Brillouin zone.

Surface plasmon dispersion for a periodic plasmonic template is obtained using analytical formulae valid for in-plane momentum matching equality between surface plasmon and the incident photons. The condition for 2D lattice can be obtained by adding appropriate Bragg components of reciprocal lattice vectors to the inplane component ($K_0 \sin\theta$) of incident photon pump (K_0), as shown in Eq. (1) (it is typically shown for 2D square lattice, where p and q are to be equal). For the hexagonal lattice the momentum matching condition can be written as in the form of Eq. (2). Surface plasmon resonance (SPR) dispersion plot for all other 2D lattices can be obtained by using the above formula but with the introduction of appropriate Bragg vectors in reciprocal space for that corresponding lattice. The symbols are defined as follows: K_0, p, q, ε_m, ε_d are

$$\left|\vec{K}_{spp}\right| = \left|K_0 \sin\theta \hat{u} + m\frac{2\pi}{p}\hat{i} + n\frac{2\pi}{q}\hat{j}\right| = \left|\vec{K}_0\sqrt{\frac{\varepsilon_m\varepsilon_d}{\varepsilon_m+\varepsilon_d}}\right|, \qquad (1)$$

$$\left|\vec{K}_{spp}\right| = \left|K_0 \sin\theta \hat{u} + m\frac{2\pi}{p}(\hat{i} + \frac{\hat{j}}{\sqrt{3}}) + n\frac{4\pi}{p\sqrt{3}}\hat{j}\right| = \left|\vec{K}_0\sqrt{\frac{\varepsilon_m\varepsilon_d}{\varepsilon_m+\varepsilon_d}}\right|, \qquad (2)$$

modulus of incident wave vector, periodicity along X-direction, periodicity along Y-direction, relative permittivity of metal and relative permittivity of surrounding dielectric, respectively; $\bar{i}$, $\bar{j}$, $\bar{u}$ are unit vectors along X-direction, Ydirection, and in plane unit vector along arbitrary direction of plasmon propagation ($K_0 \sin\theta$ is in this direction) ; m, n are integers having values ±1, ±2, ±3….; angle of incidence 'θ' is defined as in Fig. 4. The unit vector u makes an angle 'φ' with unit vector $\bar{i}$.

The surface plasmon dispersions were measured for a variety of one and two dimensional corrugated plasmonic gratings with various symmetries. Localized plasmonic resonances corresponding to flat non-dispersive modes were conspicuous by their absence. This was contrary to our computational results where the grating element showed the presence of localized surface plasmon resonances. This was recognized as due to the continuity of the gold surface although it

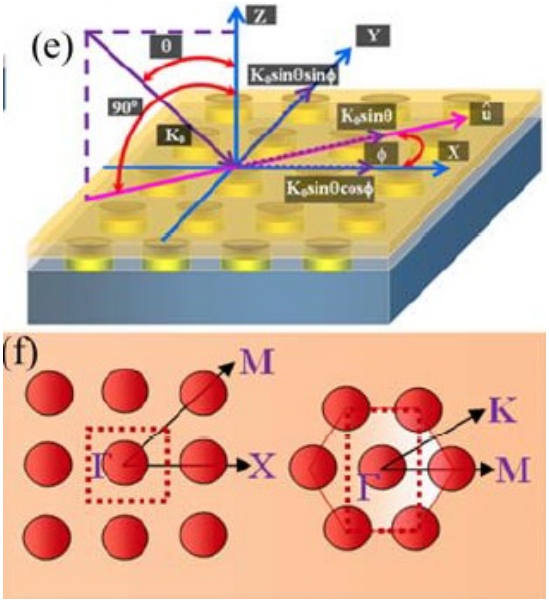

Fig. 4: (e) represents the momentum matching configuration for the incident light with wave vector K_0 (= $2\pi/\lambda$, where, λ being the incident wavelength) making an angle with the surface normal (along Z-axis or growth direction). The component $K_0\sin\theta$ which makes an in-plane angle φ with X-axis is split into components along X-axis and Y-axis. The figure (f) represents the symmetry directions for 2D square (left) and hexagonal (right) lattices in reciprocal space. Dotted boxes in respective figures represent the unit cells in real space considered for simulation. The symmetry directions are important for the understanding of in-plane momentum matching condition for the surface plasmon polariton excitation.

would be highly thickness modulated in our case. The localized plasmon resonances get highly hybridized with the propagating ones resulting in dispersive plasmons modes only. Otherwise, all the plasmon modes in the corrugated gratings could accurately be mapped onto the theoretically predicted Bragg scattered modes. This is shown in Figs. 5 and 6 for 2D corrugated gratings of square and hexagonal lattices.

Plots of the theoretical SPR dispersion can be obtained using Drude dispersive model with gold (Au) as metal having a plasma frequency of $1.35\text{x}10^{16}$ rad.s-1 and a collision frequency as $1.076\text{x}10^{14}$ rad.s-1. The refractive indices of the PMMA and photoresist can be taken as 1.4940 and 1.6241, respectively. Surface plasmon dispersions for all 2D patterned templates are investigated through broad band white light transmission measurements in the wavelength range of 450 nm to 1000 nm. It is to be noted that the dispersion features are masked by the gold intrinsic absorption below 500 nm wavelengths. In the present study, the measured dispersion range considered is between 600 to 900 nm. The details of the surface plasmon resonances are discussed in publication [1] (Attached at the end) to which the reader is referred to.

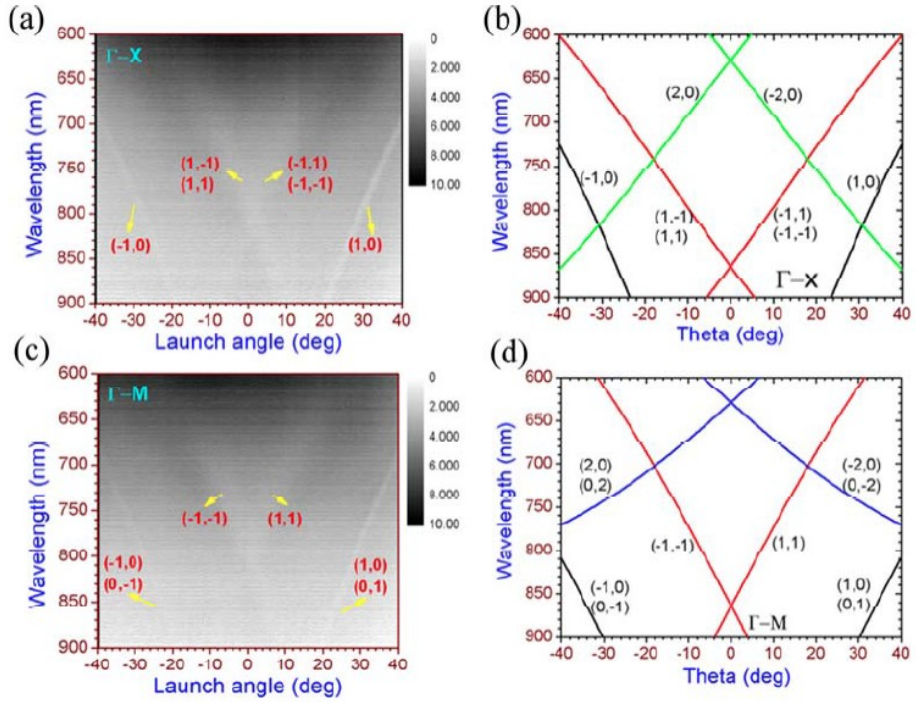

Fig. 5: Surface plots of angle dependent measured SPR dispersions (a, c) and corresponding SPR dispersion using analytical formula (b, d) for 2D square lattice along Γ-X (top-row) and Γ-M (bottom-row) symmetry directions. The periodicity of the lattice is fixed at 800 nm. Polarization of excitation light source is set accordingly (to **Γ**-X and **Γ**-M, respectively for (a) and (c)).

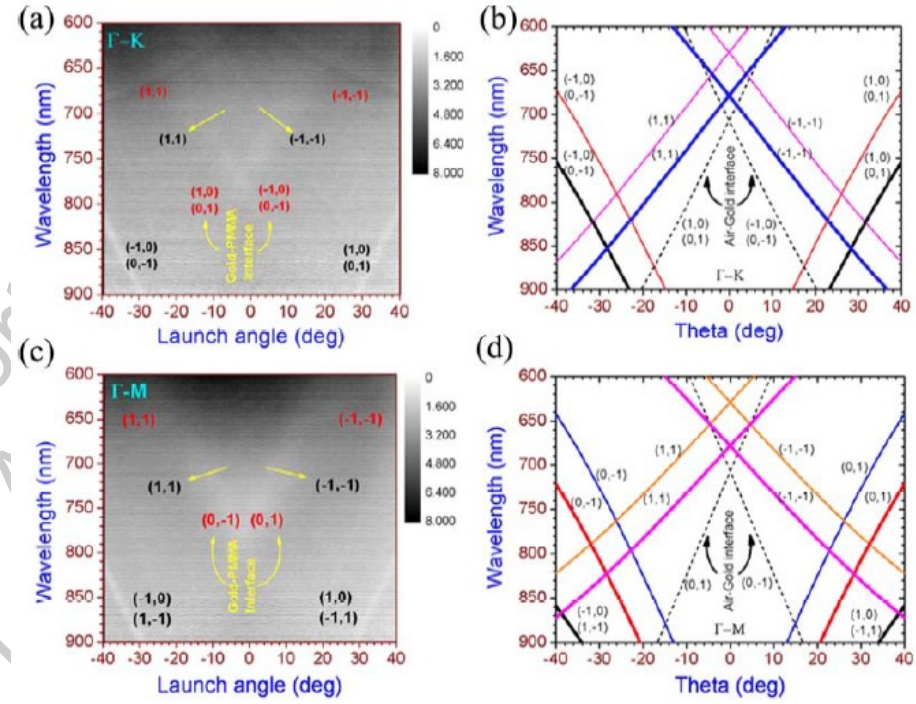

Fig. 6: Surface plots of angle dependent measured SPR dispersions (a, c) and corresponding SPR dispersion using analytical formula (b, d) for 2D hexagonal lattice along **Γ**-K (top-row) and **Γ**-M (bottom-row) symmetry directions. The periodicity of the lattice is fixed at 800 nm. Polarization of excitation light source is set accordingly (to **Γ**-K and **Γ**-M, respectively for (a) and (c)). In the analytical dispersion plots thick-lines represent the SPR at the gold-photoresist interface and thin-lines represent that for gold- PMMA interface.

Fluorescence enhancement from molecules on structured plasmonic templates

Surface enhanced fluorescence (SEF) or metal enhanced fluorescence (MEF) is a technique by which fluorescence of a fluorophore is highly enhanced by the strong interaction between near-fields and fluorophores, and through the modification of its radiative decay rate. Strong localized electromagnetic fields at the vicinity of metal nanostructures or between two metal nano-objects separated by small gap (a few nanometers) due to plasmonic excitation can resonantly interact with nearby fluorophores and modify the fluorescence decay rate (increase or decrease), resulting in enhanced or decreased fluorescence, respectively. This enhancement or quenching has been observed for a variety of material systems and also depends upon the separation between the metallic surface and the fluorophores, which can usually be manipulated as per requirements by using dielectric spacer layer. A description of the important issues and advances can be found in the introduction of publication [2] (attached at the end of the report). It is well known that nanostructures made of plasmonic materials like gold and silver can resonantly interact with radiation over a range of wavelengths from micro-scale to nano-scale through the excitation of surface plasmon resonances. These resonant interactions can result in the generation of highly enhanced and localized fields in the close vicinity of the nanostructures as well as provide for a potent manner of changing the local electromagnetic environment. The interaction of a molecule in the vicinity of these plasmonic structures, with radiation can be drastically modified by these effects.

The strong influence of the local electromagnetic near-fields and their manipulation through the structuring, the type of fluorophore, the dielectric environment, the separation between the fluorophores and metal structures, and the type of metal used are important aspects to determine the fluorescence enhancements. Hence periodic nano-patterned plasmonic templates with different geometries are promising for SEF application in view of the reproducibility that they offer. Further, due to the periodic structure, interesting interplay of Bragg scattering and the plasmonic effects can also be seen. Detailed knowledge of the plasmonic characteristics, surface plasmon dispersion and photon density of modes for these systems can result in the purposeful design of optimized structured plasmonic templates for SEF application at specific excitation wavelengths.

We studied the surface enhanced fluorescence from R6G molecules placed in a plasmonic system consisiting of corrugated gold gratings made using laser interference lithography. Due to the plasmonic coupling and consequent the large localized fields, highly enhanced fluorescence with upto 60 times enhancements are seen for efficient excitation with green radiation, while blue light excitation is not effective due to the absorption in gold. The fluorescence enhancement was found to depend highly on the period of the gratings, and the detailed correlation to the underlying plasmonic assisted excitation of the molecules was examined by experimental measurements of the surface plasmon dispersions, fluorescence images of the gratings, and detailed numerical simulations of the gratings, all of which showed large localized electromagnetic fields for certain periodicities.

The excitation of the fluorophores was performed with two Hg bands (λ_{blue} = 488 nm with FWHM 23 nm, and λ_{green} = 548 nm with FWHM 5 nm) using an Olympus BX51 fluorescence microscope through 100X objective. The fluorescence intensity was collected through the same objective in the reflection mode and coupled to an Ocean Optics HR2000+ Spectrometer having a resolution of 0.5 nm through an optical fibre. Fluorescence images of the plasmonic samples were obtained using a CCD camera coupled to the trinocular / eyepiece of the microscope.

Fluorescence images of the R6G in PMMA coated onto corrugated gratings with variety of lattice structures are shown in Fig. 2. We show the white light transmission image of a 1D grating with 1000 nm period in Fig. 2a and that of a 2D square grating with 1000 nm period in Fig. 2d. Fluorescence images of the 1D and 2D gratings when excited with green light and blue light are

shown in Fig. 2b and Fig. 2c, and Fig. 2e and Fig. 2f, respectively. It is clear that the fluorescence emission from the molecules is spatially inhomogeneous, although the distribution of R6G molecules is reasonably uniform over the entire surface. The Figures also show that fluorescence image has same symmetry as the underlying structures. The spatial inhomogeneous emission is due to spatially inhomogeneous excitation due to the plasmonic near-fields of the grating. It was noted that the fluorescence intensity typically reduces drastically in time over a few seconds immediately after the excitation radiation was switched on. This occurs due to the accumulation of R6G molecules in non-radiative triplet states – the reader is referred to publication [2] for the details of the decay of fluorescence due to accumulation in the triplet states.

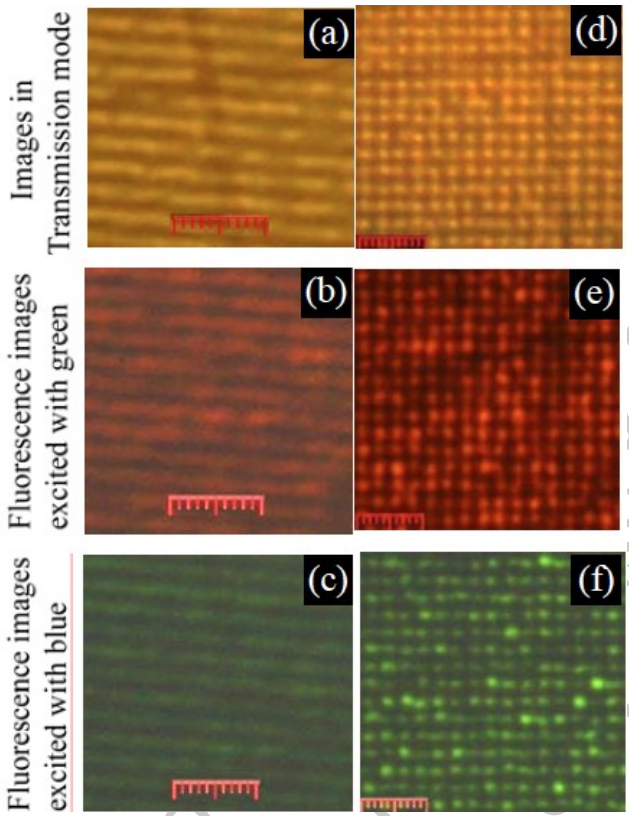

Fig. 7: Fluorescence images of few typical samples after the green and blue excitations. Red coloured fluorescence images are obtained with green excitation while dark greenish coloured fluorescence images are for blue excitation. Yellow coloured images are obtained in the transmission mode. Images are obtained on 1D gold corrugated gratings with periodicity of 1000 nm (a-c), 2D gold corrugated gratings with periodicity of 1000 nm (d-f).

Fluorescence spectra of R6G dye doped PMMA films coated on to 1D corrugated gratings having different periods (400 nm to 1100 nm) were measured for green and blue excitation light. For green excitation, the spectral shapes from all the gratings are observed to be similar in nature. Similarly, the spectra obtained with blue excitation are also similar for all the gratings, although they are necessarily different from the ones for green excitation. The primary difference is the total fluorescence intensity obtained for the different grating periods. In Fig. 8a, we show the fluorescence spectrum obtained from R6G in PMMA on corrugated grating having a period of 900 nm along with the corresponding reference spectrum obtained from plain gold coated substrate, for green excitation. Both the sample spectrum and the reference spectrum show a sharp cut-off for wavelength below 590 nm due to transmittance of the filter used. The detailed dependence of the fluorescence enhancement with the period of the corrugated gratings is shown in Fig. 8e and Fig. 8f for green and blue excitations, respectively. The dependence in Fig. 8e for green excitation shows a systematic variation in intensity, showing the strongest signals at 500 nm period and 1000 nm period. The fluorescence signal is comparably large at these two periods. It is also observed that the enhancement for these two periods is about 15 times compared to the corresponding reference signals. It is interesting that instead of single optimized period the enhancement is modulated with the period. For the blue excitation, however, the enhancements are much smaller and comparable to each other having no such clear systematic dependence. It is mentioned earlier that the spacer layer

between fluorophore and metal surface plays a crucial role for the enhancement of fluorescence. We have also checked this issue by using the optimized 1000 nm periodic structure. On the structured surface, we first put a PMMA (dielectric) spacer layer of various thicknesses and subsequently we put the R6G doped PMMA layer. Figure 9 shows the fluorescence peak intensities for green excitation with various spacer layer thicknesses. All other parameters are kept identical. It is to be mentioned that before putting R6G solution, the PMMA spacer layer coated templates were heated to 100°C for 1 minute to remove any moisture and make it uniform. The dependence shows an optimum layer thickness between 50 to 100 nm giving the highest fluorescence signal, after which it falls again with increasing spacer thickness. It is observed that below 25 nm spacer layer thickness the fluorescence intensity is almost comparable to that without the spacer layer. The highest signal obtained with the optimized spacer layer thickness is nearly 4 times as high as the signal for no spacer layer.

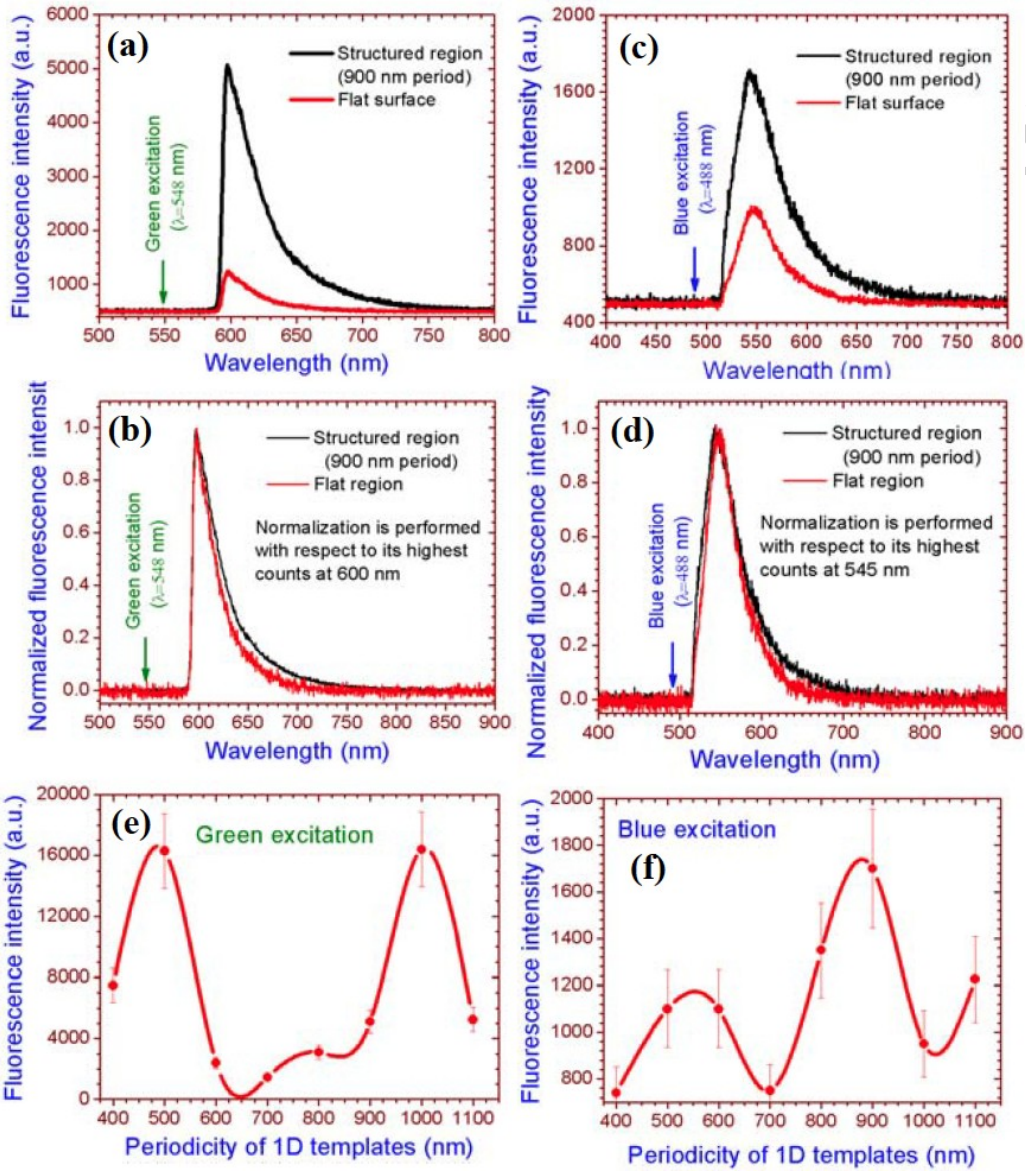

Fig. 8: Typical fluorescence spectra of 1D sample having 900 nm period after excitation with green (a) and blue (c). The spectra from the flat gold coated surface for corresponding excitations are also shown for comparison. The corresponding normalized spectrum is shown in the respective Fig. 8b and Fig. 8d. The periodicity dependent intensity profiles for green and blue excitations are shown in Fig. 8e and Fig. 8f, respectively. The profiles are obtained for 600 nm peak and 545 nm peak in the case of green and blue excitations, respectively.

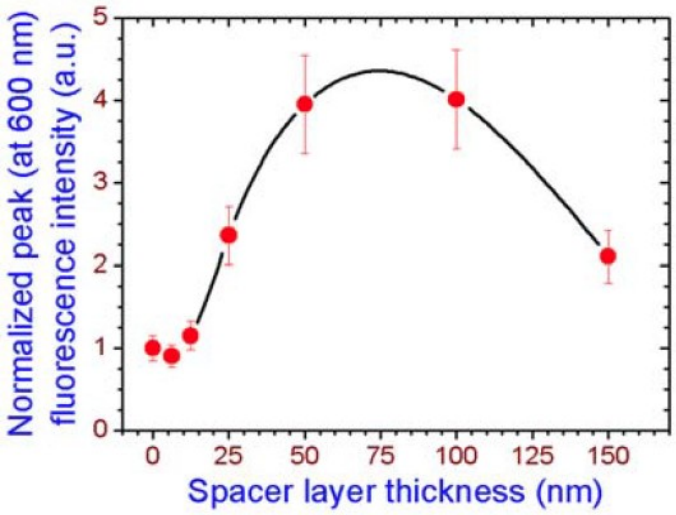

Fig. 9: Peak fluorescence intensity from R6G on 1D sample having 1000 nm period for green light excitation with respect to spacer layer thickness. The peak is normalization with the fluorescence peak counts obtained for sample with 1000 nm period and no spacer layer. The solid line is a guide to the eyes only.

The measured fluorescence enhancements could be directly correlated to the measured surface plasmon dispersions and local field enhancements for illumination of the corrugated gratings at the pump frequency as calculated by computer simulations (See Publication [2] for details). It turns out that the fluorescence is enahnced due to more efficient excitation at the periods when large local fields are caused due to surface plasmon resonance excitation by the excitation light. For the green excitation, it was clearly seen that surface plasmons could be measured over large angular ranges on gratings of certain periods which cause efficient coupling to the molecules on the surface of the grating. This causes the large dependence of the fluorescence on the period and the peaks at 500 nm period and 1000 nm periods. In comparison, gold is not a good plasmonic material at blue frequencies due to the enormous damping arising from inter-band transitions. This causes a very weak dependence of the fluorescence on the period for blue exciting light and the fluorescence is also not highly enhanced.

In general, there are two processes by which the fluorescence can be enhanced: one, by more efficient excitation that can be caused by enhanced fields of the excitation radiation; and two, by a modification of the photonic density of modes due to a modification in the electromagnetic surroundings of the molecules. Plasmonic structures can easily enhance the fields of the excitation radiation via the enhanced localized fields of the surface plasmon excitation. They can also enhance the photonic LDOS (local density of states) as in the case of nano-antennas, in which case, the radiative transitions can be strongly enhanced over the non-radiative processes in the molecules. This engineering of the molecular decay rate has also been very popular in the literature. In our case, we have effectively established that strong plasmonic coupling and consequent enhanced absorption of the pump radiation is responsible for the enhanced fluorescence with green light excitation. As the R6G molecule already has an enormous quantum efficiency (>90%) for the fluorescence in most of the host materials, large enhancements in the fluorescence are not possible by increasing the radiative transition probabilities over the non-radiative transitions. However the de-excitation of the molecules by coupling to non-radiative plasmon modes is still a possibility. In fact, this manifests in the strong quenching of fluorescence of molecules that are very close to the metallic film. It is well known that a dipole induces an oppositely oriented image dipole in perfectly conducting film. Thus, a dipole placed on a PEC (perfect electrical conductor) cannot radiate efficiently. This manifests for molecules placed directly on the gold film, which although not a perfect conductor at optical frequency, strongly quenched the emission from the molecule. The molecule is enable to radiate while the strong near-fields of the molecule couple to the non-radiative plasmonic excitation, thereby deexciting the molecules. When the molecules are, however, placed some distance away from the gold film, the emissions from the molecules and their respective

images do not destructively interfere to cancel out each other and the plasmonic enhancement to the excitation results in the strong fluorescence enhancement. Placing the molecules too far away from the surface reduces the plasmonic enhancement effect due to the rapid decay of the near field of the SPs with distance from the grating surface. This explains the optical distance (spacer layer thickness) of about 50 nm to 100 nm from the grating, when the fluorescence enhancement is most effective and largest.

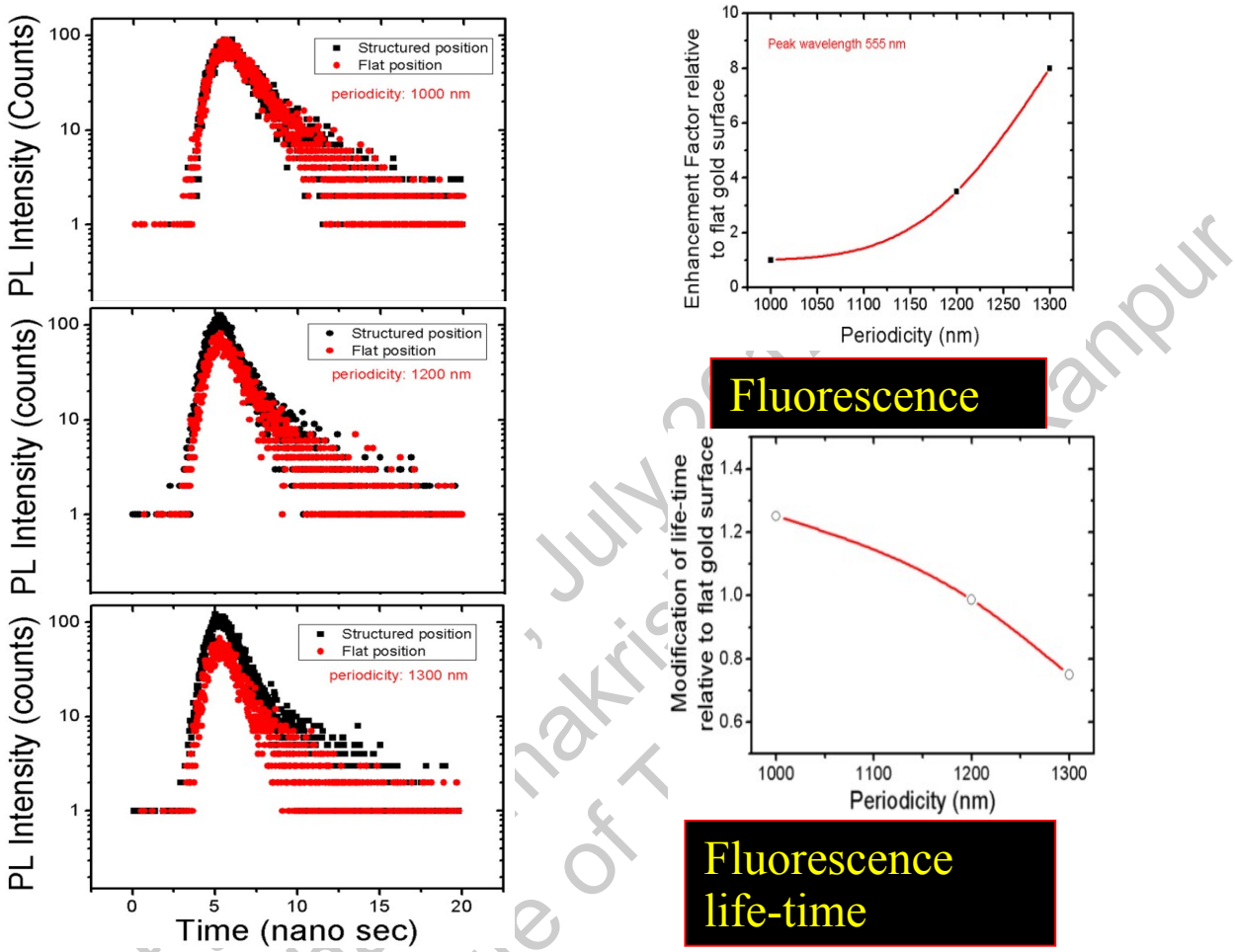

Fig. 10: Left panel – The measured fluorescence decay from the corrugated metallic gratings for three grating periods. Right panels show the fluorescence and the fluorescence lifetime as a function of the grating periods. The lines are a guide to the eyes only. While a eight fold enhancement of the fluorescence is indicated, there is correspondingly only a 20% change in the fluorescence lifetimes. This indicates that local field enhancements resulting in efficient excitation are responsible compared to the effects of changes in the photonic LDOS.

To further understand whether the radiative processes are indeed enhanced in comparison to non-radiative processes, we carried out some preliminary studies on lifetime measurement on the fluorescence from these gratings. These studies, while not complete, indicate that there can be about 20% change in the radiative life time of this R6G molecule. Fig. 10 shows the dependence of the radiative lieftimes on the period of the gratings for a few grating periods. Thus, while the corrugated gratings modulate the fluorescence emission via modified photonic LDOS, the large fluorescence enhancement for high quantum efficient molecules such as R6G is predominantly due to efficient excitation of the molecule by enhanced surface plasmon near-fields. By using a molecule like R6G with high quantum efficiency, it has been possible to study the plasmonic effects on enhanced excitation of the molecules, while not being affected extremely by the effects of modified photonic LDOS and the consequent changes in the radiative efficiencies. Finally it was seen in the computer simulations that the near-field was mostly confined to the regions at the edges

and corners, and spread over certain areas of the top-ridge surface of the metallic strips and patches. The plasmonic interaction with fluorophores in these regions will be much stronger and the strong excitation by the pump beam is expected to increase the fluorescence. Thus, fluorophores residing on the top of the structured surface feel stronger near-fields resulting in high emission compared to surrounding area. This can be seen from the fluorescence images (in Fig. 7) that mimic the geometrical structures of the original gratings. By using a molecule like R6G with high quantum efficiency, it has been possible to study the plasmonic effects on enhanced excitation of the molecules, while not being affected extremely by the effects of modified photonic LDOS and the consequent changes in the radiative efficiencies.

Surface enhanced Raman scattering from molecules on structured plasmonic templates

In our previous report we have shown how Surface Enhanced Raman Scattering can be manipulated using various plasmonic templates, especially using grating periods as major parameter. We have seen that one-dimensional (1D) grating offered significant Raman signal from the probe molecules of rhodamine 6G imbedded in PMMA (say, R6G+PMMA) compared to the signal from bare glass/fused silica substrates. The modulation or periodic enhancement of the SERS signal on plasmonic gratings was the main outcome of the results. The experimental results are also supported by electromagnetic field simulation [For details: P. Mandal and S. A. Ramakrishna, Opt Lett. **36** 2011 3705].

Continueing this study, two dimensional gratings with optimized periods were studied in detail for SERS enhancements. The results are equally impressive when two-dimensional surface nanopatterned templates (2D gratings) were used for SERS. As plasmons are sensitive to the polarization of input pump the 2D templates are considered to be superior. Additionally this system of 2D plasmonic templates can be investigated for SERS for wide angle and mixed polarization of input pump. We have also attempted to address the SERS effects by using various 2D surface patternings such as square, hexagonal, rectangle. Apart from this we employed pump power and pump wavelength dependent SERS for the optimization. Our investigation shows that SERS signal does not depend on strongly on the surface patterning structures, i.e. whether the structures are hexagonal or square or rectangle, the signal is almost comparable for each case, except a slight superiority for hexagonal structures. This is due to relatively large near-field concentration at the metallic edges and corners and probably for supporting stronger SPP (surface plasmon polariton) field (propagating). Very interesting outcome of the study is the pump wavelength dependence of the SERS signal. It is evident from the experimental results as well as simulated data that the coupling strength of input pump to the structure is very important for the enhancement of SERS. Hence, any structure which is very effective for, say, 785 nm excitation the same structure may not result good SERS for 633 nm pump. Thus the selection of input pump essentially depends on templates' structures or geometries. The optimization of SERS is therefore very wavelength specific (for details, the reader is referred to publication [1] that is attached). The excitation wavelength should also be chosen such that the particular Raman molecules do not fluoresce; otherwise the SERS signal will essentially be lost in the huge fluorescence background signal. Finally the power of the input pump also plays a role for the SERS enhancement. Lower the power the higher is the enhancement. At high power various complexities such as sample degradation, optical nonlinearity etc. come into picture, resulting less SERS effect.

A very detailed study of SERS from molecules placed on corrugated metallic surfaces with optimized periods was carried out to study the effects of structure, pump laser power and statistics from the gratings. On an average, SERS was found to enhanced by over 70 times for molecules on the gratings compared to Raman scattering from plain gold films (see Fig. 11). As the SERS from plain gold films deposited by vapor deposition methods are typically enhanced by a thousand times, it can be concluded that the SERS from the gratings are enhanced by typical factors of over 10^5. The

other interesting aspect was that the fluctuations in the SERS from various parts of the gratings was only about 20% indicating a very uniform density of hotspots. This is a very desirable aspect of these grating structures for SERS as that would result in enormous reproducibility of the SERS. Thus, our work has laid out the design principles for SERS plasmonic templates with dependable, reproducible enhancements. We expect that these SERS grating structures can easily be commercialized.

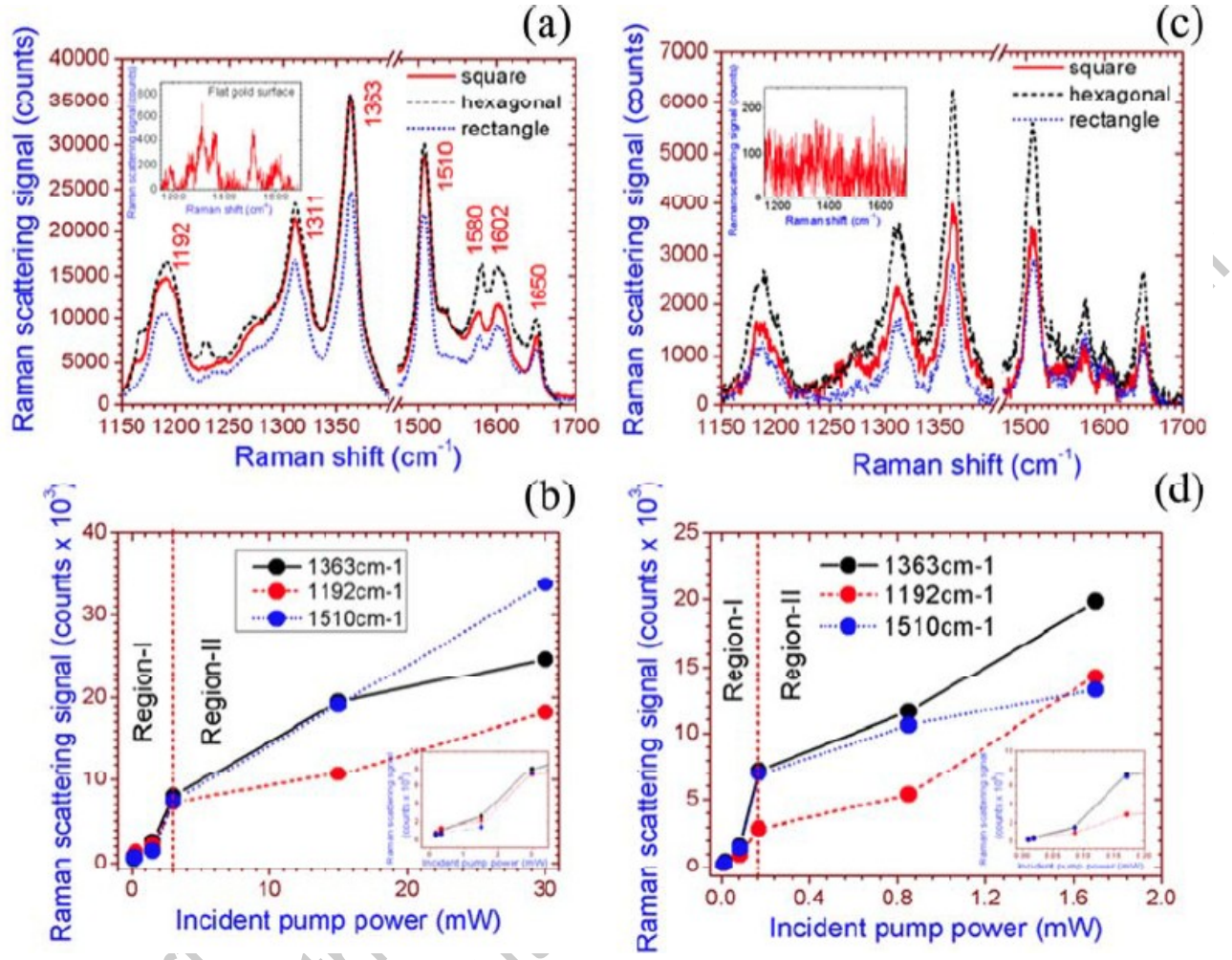

Fig. 11: Raman spectra of R6G+PMMA deposited on plasmonic templates of various patterns with fixed periodicity of 800 nm. The signal is averaged over various spots on the templates. Figures (a, b) represent the Raman plots for 785 nm pump excitation and the figures (c, d) represent the plots for 633 nm excitation. The insets in (a) and (c) represent the SERS spectrum obtained for probe molecules coated onto flat gold coated substrate. The figures (b) and (d) represent the power dependent SERS at two pump excitations (left: hexagonal lattice for 785 nm excitation, and right: square lattice for 633 nm excitation). Insets in (b) and (d) represent the expanded form of region-I and are shown for better visibility. During power dependent study the integration of Raman intensity was performed for 1 accumulation of 10 seconds with 785 nm pump laser. It is noted that the power levels only indicate the incoming laser powers and the actual intensities coupled to the sample can be different but proportional to input power.

Two studies were began that are yet incomplete, but the preliminary results are very promising.

Surface plasmons on a grating with surrounding amplifying medium

Studies on pumping of surface plasmons by an amplifying medium to extend the lifetime of surface plasmons were initiated. This results in the control of the plasmons through the pump laser. For this corrugated gratings and linear gratings of gold prepared by laser interference lithography and subsequent etching were prepared and a thin layer of PMMA containing rhodamine 6G at larger concentration levels of about 10^{-4} molar was deposited on the gratings. By shining a diode pumped solid state laser with about 30 mW, the Rhodamine 6G dye could be excited and conditions for laser gain are prepared.

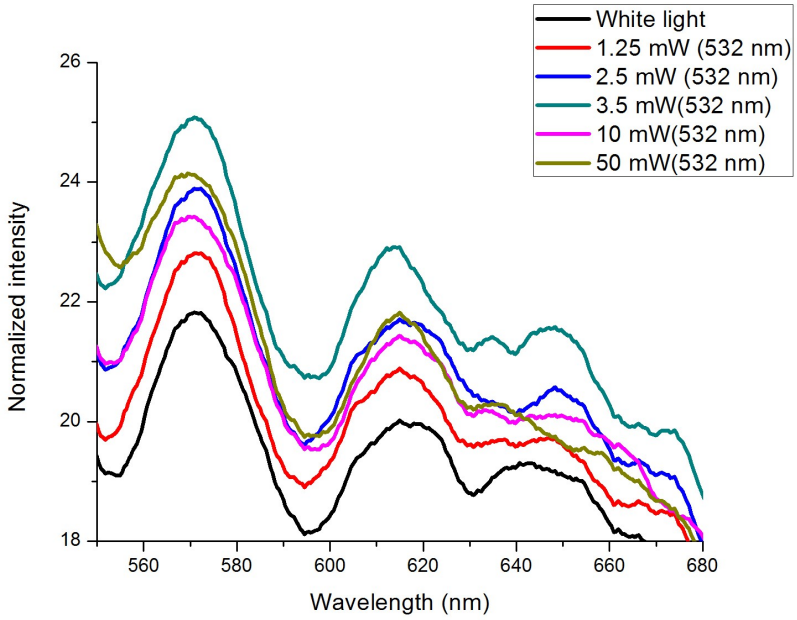

Fig. 12: The transmission of white light through a corrugated gold grating with a 20nm layer of 100 micromolar rhodamine 6G in PMMA on the grating, as a function of the wavelength and power of a 532 nm laser co-incident with the white light spot. The 532 nm laser is absorbed by the R6G creating conditions of gain in the medium for the wavelengths 560 nm to 630 nm. The overall increase in transmission due to the stimulated emission is clear, while there are interesting spectral changes at about 590 nm and a split plasmon peak at 630 nm. There could be various mechanisms for these changes which are being investigated.

White transmission studies through these gratings with and without the pump laser being incident on the films were recorded. Preliminary findings indicate that the transmission in the presence of the laser is enhanced within the surface plasmon absorption dip when the surface plasmon dip lies within the fluorescence band of R6G [560 nm to 620 nm]. Such a transmission is shown in Fig. 12, for various intensities of the pump laser. Further studies in this respect are in progress.

Non-linear transmission measurements on multi-layered plasmonic structured films

The multi-layered plasmonic structured films with alternating layers of R6G doped PMMA and gold of 20 – 30 nm each were studied for transmission. A study of the intensity dependent transmission has indicated that the system shows signs of reverse saturable absorption at 532 nm- Absorbance of the film increases with the intensity of the light. These studies, however, need

confirmation and apart from a brief mention, it does not merit a substantive discussion at this stage. The system is, however, very promising from the viewpoint of non-linear plasmonics. More studies are at present being carried out on this system.

Future aspects:

The project has opened up several new possibilities. Design of plasmonically enhanced templates for fluorescence and SERS gives rise to applications in biosensing and chemical sensing applications. The study has shown the clear correlation between the enhanced localized near-fields due to propagating surface plasmons and the enhancement in fluorescence and SERS. The uniform enhancements and uniform hot-spot densities in our systems indicates that highly reproducible sensing capabilities will present themselves. These are the need of the hour for sensing applications. These gratings can easily be commercialized and taken up for production. The studies on surface plasmons in systems with laser amplification (gain) and nonlinear absorption in dye-doped multi-layered plasmonic templates represent very interesting future possibilities. One aspect of the control on the plasmonic system is through its lifetime and potential applications for plasmonics present themselves in this regard. The possibility of saturatble and reverse saturable absorptions with very low intensities and fast responses can give rise to many potential devices.

Deviations from the original objectives with reasons

There were no deviations from the original objectives. Studies on the multi-layered plasmonic templates could not be completed due to insufficient time and are presently ongoing. The results of these studies will be published in the future and appropriate acknowledgment of the AOARD grant that contributed to their development will be given.

Other personnel involved with the Project:

1. Dr. Prasanta Mandal, Post-doctoral Fellow, Project Scientist (employed by this project)
2. Mr. Amitabh Nandi, Ph.D. Student, Physics department, IIT Kanpur (not funded by this project)
3. Mr. Prince Gupta, Ph.D. Student, Physics department, IIT Kanpur (not funded by this project)

S Anantha Ramakrishna

Dr. S. Anantha Ramakrishna
(Principal Investigator)

Propagating surface plasmon resonances in two-dimensionally patterned gold-grating templates and surface enhanced Raman scattering

P. Mandal[1,a)], A. Nandi[1], and S. Anantha Ramakrishna[1,2]

[1]Department of Physics, Indian Institute of Technology Kanpur, Kanpur-208016, India
[2]Indian Institute of Science Education and Research Mohali, Knowledge City at Sector 81, Mohali, India

ABSTRACT
Surface enhanced Raman scattering (SERS) from Raman active rhodamine-6G probe molecules is investigated on two-dimensionally patterned gold-grating templates having submicron periodicity of 800 nm. Two-dimensional surface nano-patterning in the form of square, hexagonal and rectangle has been obtained through cost effective laser interference lithography. We find a reproducible SERS enhancement of the order of 10^5 on these nano-patterned plasmonic templates, showing a slight superior result on hexagonal patterned templates. Strong localized near-fields due to surface plasmon resonance (SPR) lead to such an enhancement. We find evidence for good correlation in the SPR excitation and enhanced Raman scattering through experimental investigation by using different Raman pump excitation wavelengths of 785 nm, 633 nm and 514 nm, and different pump powers. The results are strongly supported by computer simulations of the electromagnetic fields at the pump wavelengths. Our results demonstrate that an optimized selection of the structure and pump excitation wavelength is necessary for good SERS signal.

Keywords: Surface enhanced Raman scattering, surface plasmon, laser interference lithography
[a)]Corresponding author: Tel: +91 512 259 6601
Fax: +91 512 259 0914
Email: pmandal@iitk.ac.in

I. INTRODUCTION

In the past two decades, Surface Enhanced Raman Scattering (SERS) has been investigated extensively for its high sensitivity in detecting trace molecules, for molecular vibrational information, and sensitive bio-molecular detection.[1-6] Raman scattering efficiency drastically gets enhanced for rough metallic surfaces due to the strong near field localization and enhancement at the metallic sharp edges or between two closely spaced metallic nano-objects.[7-18] A variety of patterned templates having specific metal nanostructures, such as nanorods, hemispheres, nanocrescent arrays, nanorings, dimers, nanoprisms, nanocrystals, nanoparticles in a periodic template and nanogratings[19-28] have been studied to optimize SERS and understand the origin of the large local fields. The surface plasmon modes associated with the metallic nanostructures have been found to enormously contribute to the SERS by giving rise to large localized electromagnetic fields. Surface plasmon electromagnetic modes are tightly bound to the metallic surface and decay evanescently from the surface.[29] Fig. 1 schematically shows this nature of surface plasmons on a metallic surface. Interestingly, in a given area of the pump beam, the density of regions with concentrated near-fields or 'hot-spots' is a prime contributor to SERS. Therefore, a high density of hot-spots is always required to obtain SERS in a reproducible manner on good plasmonic templates. In this context, tip-enhanced Raman scattering (TERS) has been very promising as the sharp metallic tip essentially represents the local host of high concentrated near-fields, and has been investigated by various researchers.[30,31] However, the use of tip enhanced SERS is limited by the formation of a single hot-spot between the tip and the probe molecules. Alternatively, by structuring a metal surface in a regular periodic manner with small periodicity, one can reproducibly produce hot-spots. Edges and corners of a metallic strip typically focus the spatial near fields. Therefore, planar gratings or patch like patterns are studied to optimize SERS.[10,23,28] Plasmonically resonant two-dimensional (2D) patterned templates can also be considered to be superior to one-dimensional (1D) counterparts as the resonant plasmonic modes in 2D structures can easily be excited using TM, TE or mixed TM-TE polarized input pump. Hence, an unpolarized pump laser can effectively excite the plasmonic modes and give rise to SERS from probe molecules placed upon the 2D structures.

Fabrication of small periodic grating structures (<200 nm pitch) needs the involvement of expensive instrumentation such as e-beam lithography, focused ion-beam milling or by UV photolithography with expensive UV optics and UV lasers. Nanoimprint lithography can also be considered as an effective and simple tool for quick reproduction of nanopatterns.[32] However, expensive instrumentations, in this case, are needed for the design of master die. Alternatively through chemical approaches, small metal spheres can be arranged on a preformed template in a regular fashion and achieved very small gaps (<25 nm) in between them in order to obtain large localized fields in the nano-gaps.[24] Metallic/ metallo-dielectric gratings are promising in this regard and have been used for reproducible SERS.[10,23,33,34] In a recent report[35] it has been shown that SERS can be manipulated by changing the periods of metallo-dielectric sub-micron gratings. These gratings with moderately high pitches ranging from 300 nm to about few microns

can easily be fabricated using low-cost visible frequency laser interference lithography (LIL) technique[36,37] within very short time. From our previous study and existing literatures, the excitation of resonant plasmonic modes has been shown to lead large SERS (enhancement factors:~10^3 - 10^8) when compared to the Raman signal from neat solutions.[38] In this report we present an exhaustive study showing the effects of 2D periodic patterning affects the SERS from molecules placed on these plasmonic templates. A variety of regularly patterned gold sub-micron 2D grating templates fabricated using laser interference lithography (LIL) are used as plasmonic templates for SERS measurements. Rhodamine-6G (R6G) doped poly methyl methacrylate (PMMA) is used as SERS probe. The SERS mechanism in relation to the enhanced near-fields has been addressed through experimental investigations by considering various 2D surface lattice patterns, pump wavelengths and pump powers. A correlation is demonstrated between the measured dispersion of surface plasmon modes, near-field excitation and SERS using analytical formulation and Finite Difference Time Domain (FDTD) computations.

II. EXPERIMENTAL & FABRICATION DETAILS

Thoroughly cleaned glass plates (1 mm thick) are used as substrates onto which photoresist (ma-P 1205 from 'micro resist technology', Germany) was spin coated at 3000 rpm, and prebaked at 80^0C for 1 minute. The photoresist coated glass plates were subsequently exposed to interference patterns produced by a single longitudinal mode 473 nm wavelength diode laser typically for 20 minutes. Double exposures (first exposure of 10 minutes followed by a sample stage rotation of desired angle and second exposure of 10 minutes) were used for generating 2D grating templates. To generate square and hexagonal patterns the sample stage was rotated by 90^o and 60^o, respectively. The periodicity for these 2D grating templates was fixed at 800 nm for highest Raman signal at 785 nm pump wavelength.[35] For rectangular patterns, we changed the period of the interference pattern to 1300 nm before the second exposure. The exposed photoresist films were developed using a standard developer which resulted in periodically patterned photoresist film on the glass substrates. Finally, a thin layer (40 nm) of gold was thermally evaporated onto these patterned surfaces. The typical fabrication process of plasmonic templates through LIL and post development evaporation of metal is shown in Fig. 1. Atomic force microscope (Agilent PicoSPM II) was used to measure the depth of the patterns. Surface patterns were imaged through an Olympus BX51 microscope in bright-field and dark-field configurations.

Angle resolved white light transmission measurement (using home built spectroscope) was performed to study surface plasmon resonance dispersion in the range of -40 degree to +40 degree with a step of 0.2 degree. Tungsten halogen lamp (100 watt) was used as the white light source. The final collimated beam (~1 mm) was allowed to fall onto samples mounted on a computer controlled goniometer stage. The transmitted beam was collected through an optical fibre and the spectra were recorded using 'Ocean Optics' spectrometer (model: HR2000+ having resolution of 0.5nm) in the wavelength range of 400-1000nm. A polarizer was used to adjust polarization direction to match sample orientation for TM/TE (transverse magnetic/transverse electric) configurations.

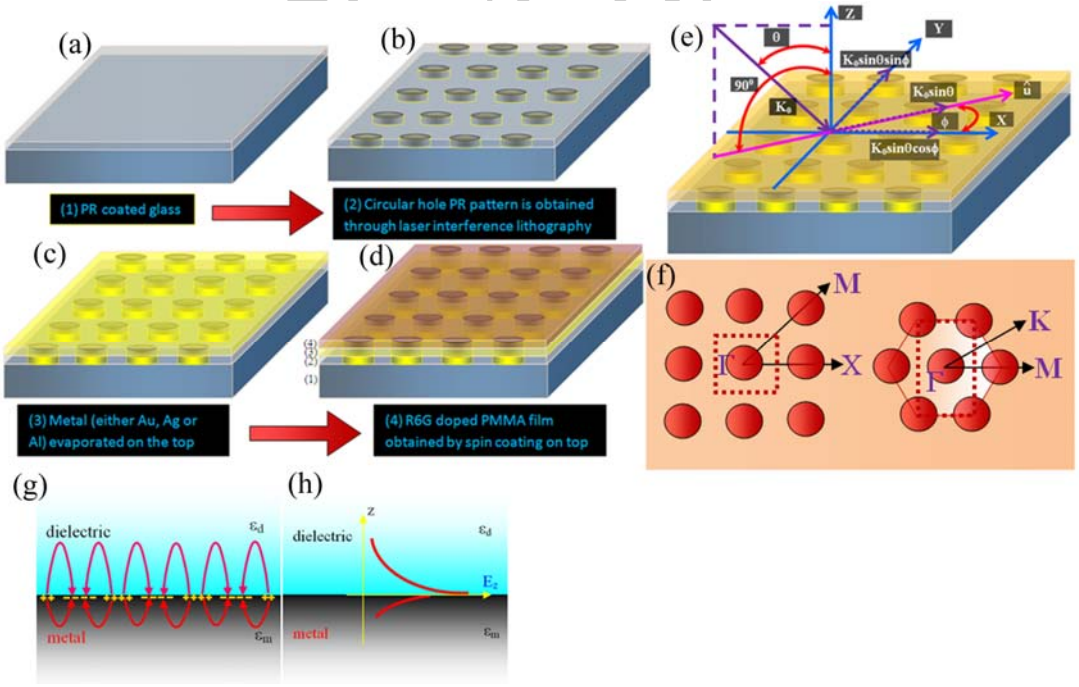

FIG. 1. Typical fabrication steps involved to generate plasmonic templates through laser interference lithography and post development evaporation of metal films onto the structured surfaces. The figures (a-d) represent the steps: (a) glass substrate coated with photoresist, (b) the photoresist coated glass substrates exposed to laser interference pattern and developed in standard developer

leaving photoresist pattern on glass, (c) metal (gold) is thermally evaporated subsequently onto the structured surface resulting in modulated metal surface on top, and finally (d) the probe molecules are spin coated onto the top of the modulated metal surface. Figure (e) represents the momentum matching configuration for the incident light with wave vector K_0 (= $2\pi/\lambda$, where, λ being the incident wavelength) making an angle with the surface normal (along Z-axis or growth direction). The component $K_0\sin\theta$ which makes an in-plane angle ϕ with X-axis is split into components along X-axis and Y-axis. The figure (f) represents the symmetry directions for 2D square (left) and hexagonal (right) lattices in reciprocal space. Dotted boxes in respective figures represent the unit cells in real space considered for simulation. The symmetry directions are important for the understanding of in-plane momentum matching condition for the surface plasmon polariton excitation. The numbers 1, 2, 3, 4 labeled in the figure (d) represent substrate, PR pattern, evaporated metal and R6G doped PMMA film, respectively. Figures (g, h) represent SPR excitation (left) and decay of evanescent electric field (right) in either side of the dielectrics' interface.

Raman active R6G molecules (52 μmol) in PMMA (chlorobenzene solution of PMMA was purchased commercially from MICROCHEM, Germany) were spin coated onto the plasmonic templates which resulted in ~ 50 nm film thickness. In this configuration it can be ensured that the SERS signal is primarily contributed by electromagnetic contribution while minimizing the chemical effects (R6G not adsorbed on the metal surface). It can be ascertained that while the above statement is true for R6G it can be relaxed for PMMA which is also Raman active. We also ascertain that the regions of high concentrated globules with agglomerated R6G onto the structured region are strictly avoided. Raman measurements were performed using a Renishaw inVia Raman spectrometer typically with 785 nm laser at 3 mW input power (the actual power coupled to the sample can be different but proportional to input power). The laser was focused through 50X objective (Numerical aperture: 0.75 and probe beam size ~ 5 micrometer) and back scattered signal was collected through the same objective. The intensity was integrated over 2 accumulations of 20 seconds each (unless otherwise stated). Other pump wavelengths were also used and the detailed parameters are described in the respective section. It is to be mentioned here that although the actual experimental investigation (SERS) has also been made for 514 nm pump laser but the simulation is not presented in this report as the fluorophores molecules are highly fluorescent at this excitation wavelength. The Raman signal appeared to be very weak with a highly fluorescent background.

III. EXPERIMENTAL RESULTS

We investigate SERS on 800 nm periodic structures having 2D patterns such as square arrays, hexagonal and rectangular patterns. Surface topologies of the fabricated structures are studied through optical microscope in the reflection mode with bright-field and dark-field configurations. Figure 2 (a-f) shows microscope images of some 2D square, hexagonal and rectangular patterned templates with a fixed period of 800 nm (for the rectangular pattern one arm is 1300 nm in length). The top (a-c) and middle (d-e) rows show the bright-field and dark-field images, respectively. All the images show nearly 50:50 duty cycle (feature size and separation between two objects are almost same). The insets in the top row images represent the corresponding fast-Fourier transform (FFT) images signifying the long-range order and the lattice configuration in reciprocal space. Figure (g) shows atomic force microscope image of a typical 800 nm periodic 2D square pattern. The figure (h) represents the depth profile of the corresponding AFM image (note: green line) showing an average depth of about 200 nm. The inset in (g) shows the FFT of the square lattice.

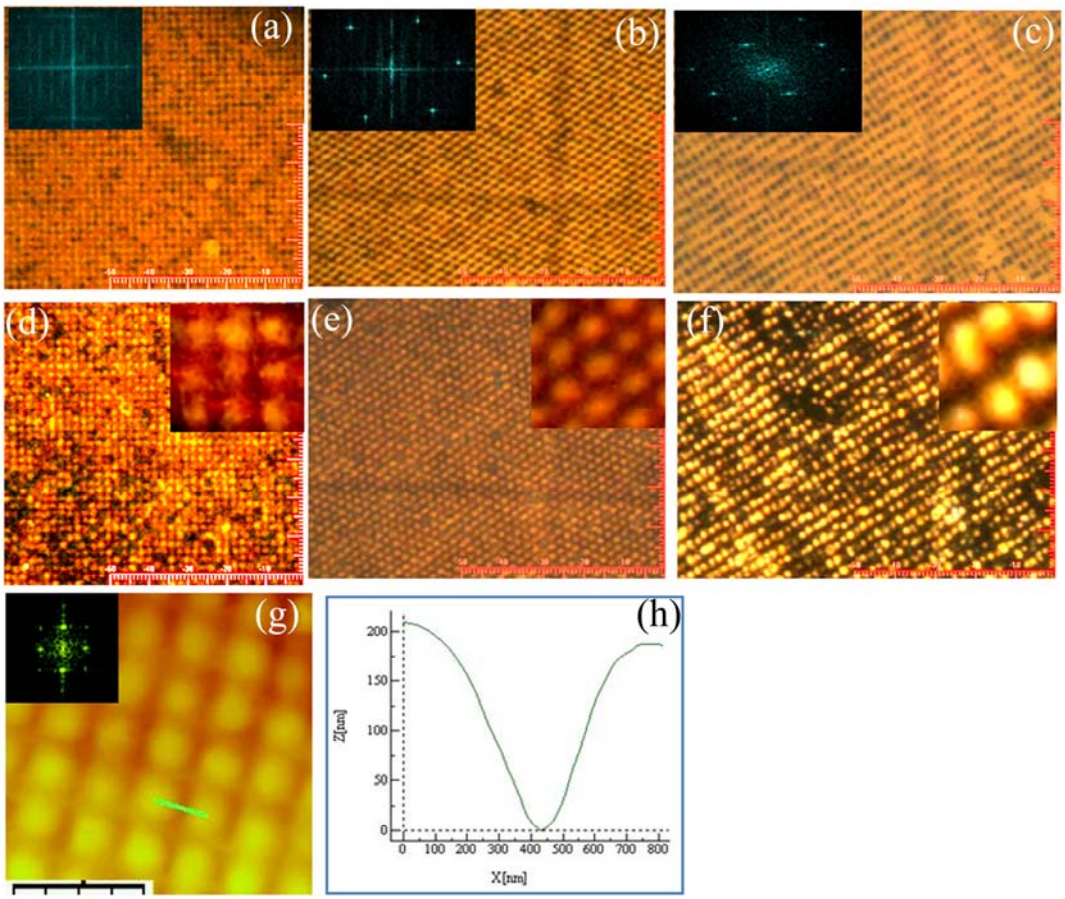

FIG. 2. Bright field microscope images of various plasmonic templates having 2D periodic patterns: square (a), hexagon (b) and rectangle (c). Corresponding dark-field images (column wise) are shown in figure (d-f). Dark-field images are to show the edge scattering effect. False colour is for clarity only. Horizontal scale bar in the spectroscopic images represents 18.9 μm. Insets in top row represent the fast-Fourier-transform of the corresponding image while that in the middle-row represent a magnified view (not in scale) of a small part of the corresponding dark-field images. Atomic force microscope image (inset: fast-Fourier transform) of a typical 800 nm periodic 2D square pattern and its corresponding depth profile are shown in figures (g) and (h), respectively.

A. Measurements of surface plasmon dispersion

Surface plasmon dispersion for a periodic plasmonic template is obtained using analytical formulae valid for in-plane momentum matching equality between surface plasmon and the incident photons.[29] The condition for 2D lattice can be obtained by adding appropriate Bragg components of reciprocal lattice vectors to the inplane component

(K_0sinθ) of incident photon pump (K_0), as shown in Eq. (1) (it is typically shown for 2D square lattice, where p and q are to be equal). For the hexagonal lattice the momentum matching condition can be written as in the form of Eq. (2). Surface plasmon resonance (SPR) dispersion plot for all other 2D lattices can be obtained by using the above formula but with the introduction of appropriate Bragg vectors in reciprocal space for that corresponding lattice. The symbols are defined as follows: K_0, p, q, ε_m, ε_d are

$$\left|\vec{K}_{spp}\right| = \left|K_0 \sin\theta \hat{u} + m\frac{2\pi}{p}\hat{i} + n\frac{2\pi}{q}\hat{j}\right| = \left|\vec{K}_0\sqrt{\frac{\varepsilon_m\varepsilon_d}{\varepsilon_m+\varepsilon_d}}\right|, \quad (1)$$

$$\left|\vec{K}_{spp}\right| = \left|K_0 \sin\theta \hat{u} + m\frac{2\pi}{p}(\hat{i} + \frac{\hat{j}}{\sqrt{3}}) + n\frac{4\pi}{p\sqrt{3}}\hat{j}\right| = \left|\vec{K}_0\sqrt{\frac{\varepsilon_m\varepsilon_d}{\varepsilon_m+\varepsilon_d}}\right|, \quad (2)$$

modulus of incident wave vector, periodicity along X-direction, periodicity along Y-direction, relative permittivity of metal and relative permittivity of surrounding dielectric, respectively; $\hat{i}$, $\hat{j}$, $\hat{u}$ are unit vectors along X-direction, Y-direction, and in plane unit vector along arbitrary direction of plasmon propagation (K_0sinθ is in this direction) ; m, n are integers having values ±1, ±2, ±3….; angle of incidence 'θ' is defined as in Fig. 1. The unit vector $\hat{u}$ makes an angle 'ϕ' with unit vector $\hat{i}$. Plots of the theoretical SPR dispersion can be obtained using Drude dispersive model with gold (Au) as metal having a plasma frequency of $1.35\text{x}10^{16}$ rad.s^{-1} and a collision frequency as $1.076\text{x}10^{14}$ rad.s^{-1}.[39] The refractive indices of the PMMA and photoresist can be taken as 1.49[40] and 1.62[41], respectively.

Surface plasmon dispersions for all 2D patterned templates are investigated through broad band white light transmission measurements in the wavelength range of 450 nm to 1000 nm. It is to be noted that the dispersion features are masked by the gold intrinsic absorption below 500 nm wavelengths. In the present study, the measured dispersion range considered is between 600 to 900 nm. We sequentially discuss the experimental SPR dispersion for square pattern and hexagonal pattern in the coming section.

Experimental measured dispersion of surface plasmon on a 2D square lattice along the Γ-X and Γ-M symmetry directions are shown in Fig. 3. The corresponding theoretical predictions are also shown. The top-row (a, b) represents SPR dispersions for Γ-X direction while bottom row (c, d) represents that for Γ-M direction. The plots of the measured dispersions show SPR excitation in the range of 600 nm to 900 nm due to various Bragg modes. The modes are easily identified from the corresponding theoretical plots for the corresponding symmetry directions.

In the experimental surface plasmon resonance dispersion along the Γ-X direction (figure 3a), the (1,0) Bragg mode is observed to be very strong with narrow width while degenerate (-1,1) and (-1,-1) modes are also observed to be strong but with significant broadening. No other modes are visible in this range of interest. The modes along the Γ-M direction (figure 3c) are identified to be degenerate (1,0) and (0,1) modes, and non-degenerate (1,1) and (-1,-1) modes. The widths of these modes are seen to be similar as in the case of Γ-X symmetry direction. These measured dispersions in both the cases (Γ-X and Γ-M) are observed to be similar. The crossing of (1,±1) and (-1,±1) for Γ-X, and (1,1) and (-1,-1) for Γ-M symmetry directions are observed to appear around 800 nm. It is to be mentioned that the experimental resonant point (at θ = 0 for square lattice in Γ-X and Γ-M directions) slightly differs from that seen from theoretical plots. In theoretical plots the top PMMA layer is assumed to be infinite, which is, in fact, not true as the top PMMA layer is only about 50 nm thick. Plasmon spatial fields' extension can exceed the thickness of PMMA layer; therefore, consideration of finite thickness of the top dielectric layer is necessary for the better fit with the experimental data. The broadening of Bragg mode is due to strong interaction of propagating plasmon resonance with localized plasmon resonance. It is noted that the dispersionless localized plasmon modes or theta independent modes are not clearly visible in the dispersion spectra. This observation signifies the dominating role of propagating SPR in the system. The huge local field is thus due to resonance of propagating SPR with localized SPR, having dominating contribution from propagating SPR.

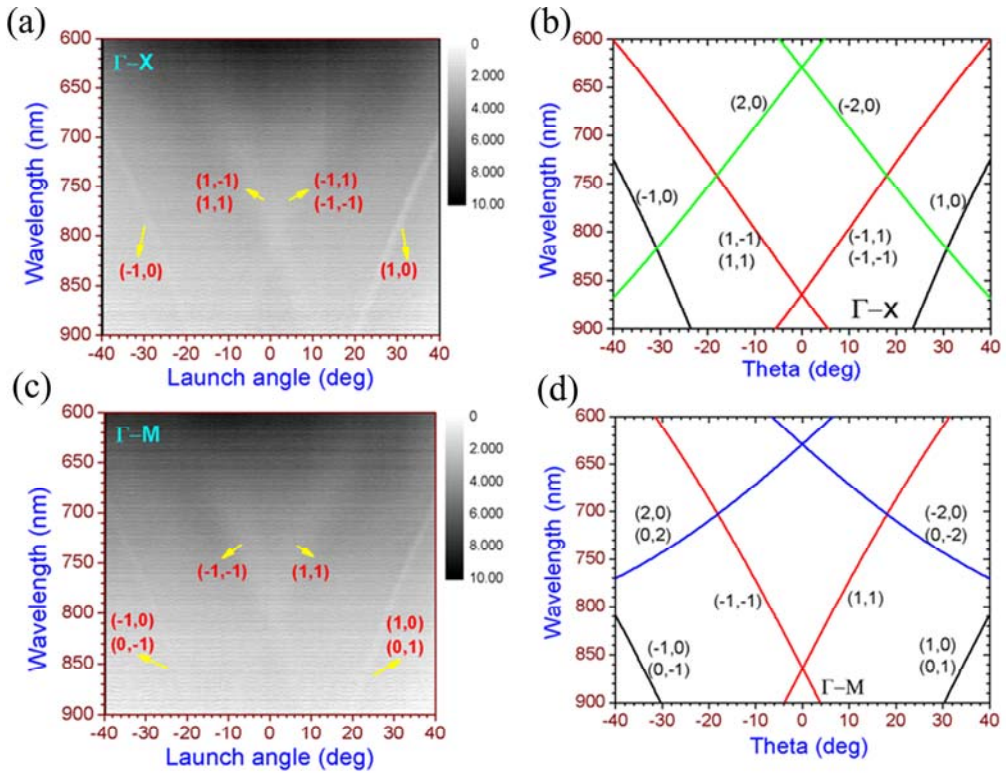

FIG. 3. Surface plots of angle dependent measured SPR dispersions (a, c) and corresponding SPR dispersion using analytical formula (b, d) for 2D square lattice along Γ-X (top-row) and Γ-M (bottom-row) symmetry directions. The periodicity of the lattice is fixed at 800 nm. Polarization of excitation light source is set accordingly (to Γ-X and Γ-M, respectively for (a) and (c)).

SPR dispersions for hexagonal patterned templates along the Γ-K and Γ-M symmetry directions are shown in Fig. 4. The modes along Γ-K and Γ-M symmetry directions are identified by comparing with the respective dispersions obtained through analytical formulation ((b, d) of Fig. 4). The deviation of experimental resonant points from analytical plots is due to the finite thickness of PMMA layer as has been mentioned earlier. The experimentally observed modes along Γ-K symmetry direction are found to be similar to that for Γ-M symmetry direction. The degenerate modes (1,0) and (0,1), and (-1,0) and (0,-1) for Γ-K are observed to be broad. Similar broad (0,1) and (0,-1) modes are also observed for Γ-M symmetry direction. Scattering due to local defects in the structures and strong interaction between propagating and localized plasmons cause this broadening as has already been mentioned earlier, although other possibilities such as coupled

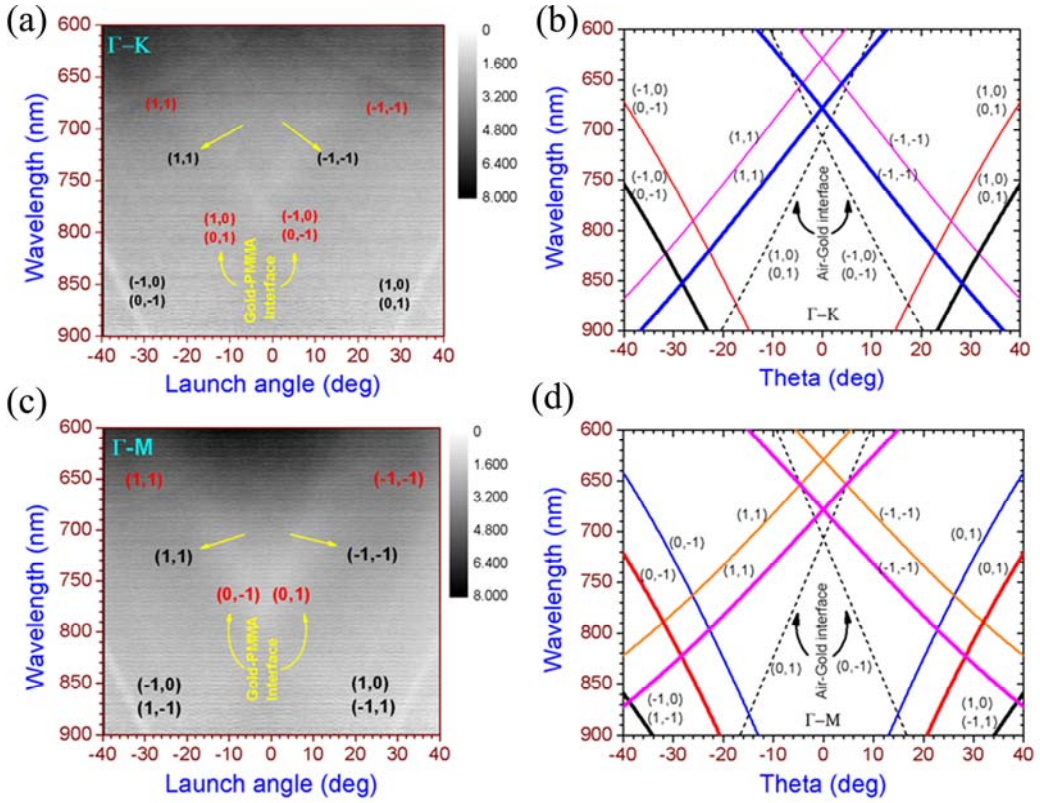

FIG. 4. Surface plots of angle dependent measured SPR dispersions (a, c) and corresponding SPR dispersion using analytical formula (b, d) for 2D hexagonal lattice along Γ-K (top-row) and Γ-M (bottom-row) symmetry directions. The periodicity of the lattice is fixed at 800 nm. Polarization of excitation light source is set accordingly (to Γ-K and Γ-M, respectively for (a) and (c)). In the analytical dispersion plots thick-lines represent the SPR at the gold-photoresist interface and thin-lines represent that for gold-PMMA interface.

surface plasmon resonances (SPRs) existing at the metal-photoresist and metal-PMMA interfaces cannot be ruled out completely. This is due to the fact that the refractive indices for both the dielectrics are close to each other. The features highly boost the local-fields enhancement and the resonant interaction with probe leads to highly enhanced SERS. It is interesting to note that the zero crossing point of various SPR modes observed experimentally arises at wavelength around 800 nm for these periodic structures which is very closure to the excitation wavelength (785 nm). These observations give strong evidence for the strong coupling of propagating and localized modes at the pump energy.

B. SERS Measurements

With this background we now present the measured SERS data for probe molecules deposited onto 2D patterned gold templates. We investigated SERS on three types of lattices: square, hexagonal and rectangular with same period of 800 nm (except that one side of the rectangular patch has length of 1300 nm). The pump wavelengths used were 785 nm, 633 nm and 514 nm. The SERS enhancement is compared with that from a flat metal (gold) coated surface deposited by thermal evaporation.

Raman spectra (averaged over various spots) from R6G+PMMA probe molecules spin coated on to 2D patterned templates are shown in Fig. 5. The signals are collected in identical conditions and averaged over different spots in all the cases. The background corrected spectra are shown in the range of 1150 cm^{-1} to 1700 cm^{-1} for the excitation at 785 nm (left) and 633 nm (right). The samples in both the cases show strong peaks associated with various Raman transitions of the R6G probe molecules. The peaks can be assigned to various transition levels according to existing literatures.[9,42,43] In brief, peak at 1192 cm^{-1} is associated with CH in–plane deformation of R6G, strong peaks at 1311 cm^{-1} and 1363 cm^{-1} are associated with stretching vibration of CC and CN of R6G, the other strong peak at 1510 cm^{-1} is due to the C–C stretching of R6G, and the prominent but weaker peaks at 1580 cm^{-1}, 1602 cm^{-1} and 1650 cm^{-1} are associated with the CC stretching of R6G.

Raman signal, in the case of 785 nm excitation, shows an average enhancement of the order of 75 for different peaks compared to the signal obtained from probe molecules on a plain gold surface. This enhancement is

nearly equal for square and hexagonal lattices, whereas, for rectangular lattice it is slightly less. Variation in the enhancement factor for different peaks of a

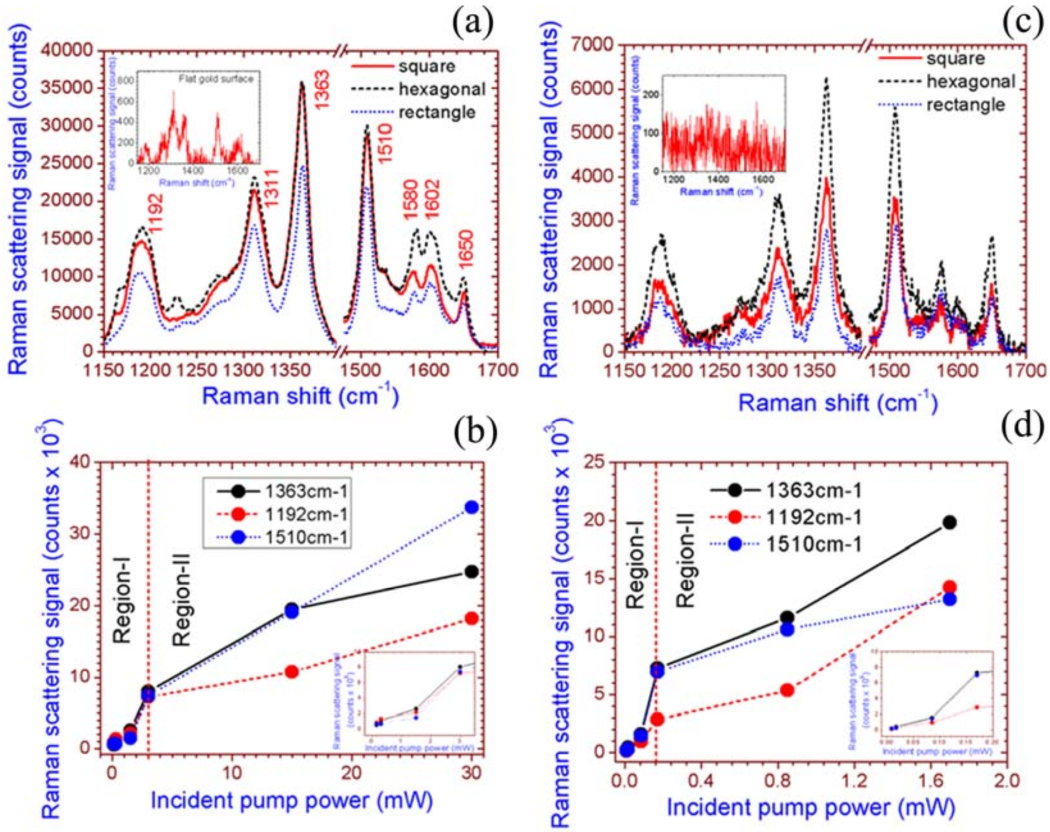

FIG. 5. Raman spectra of R6G+PMMA deposited on plasmonic templates of various patterns with fixed periodicity of 800 nm. The signal is averaged over various spots on the templates. Figures (a, b) represent the Raman plots for 785 nm pump excitation and the figures (c, d) represent the plots for 633 nm excitation. The insets in (a) and (c) represent the SERS spectrum obtained for probe molecules coated onto flat gold coated substrate. The figures (b) and (d) represent the power dependent SERS at two pump excitations (left: hexagonal lattice for 785 nm excitation, and right: square lattice for 633 nm excitation). Insets in (b) and (d) represent the expanded form of region-I and are shown for better visibility. During power dependent study the integration of Raman intensity was performed for 1 accumulation of 10 seconds with 785 nm pump laser. It is noted that the power levels only indicate the incoming laser powers and the actual intensities coupled to the sample can be different but proportional to input power.

spectrum for a sample is observed indicating the effect of SERS.[35] It is the plasmon resonance which plays the crucial role for this variation as the condition for resonance depends strongly on the pump wavelength. The Raman peaks observed from the probe molecules on to flat metal surface clearly show the weak intensity behaviour but with distinct features. The results indicate that the flat metal surface is not very smooth and the weak excitation of localized plasmon may arise due to scattering by roughness. The Raman enhancement in the case of 633 nm excitation is of the order of 50. The variation in the enhancement for different patterned templates is reflected in the figure. The peaks are very well resolved, especially in the high frequency region, which is relatively less distinct in the case of 785 nm excitation. However, the reference signal or the signal from the flat surface is weak and the peaks are not clearly resolved. The superiority of the square and the hexagonal patterns over the rectangular pattern is clearly once again reflected from the Figures. Moreover, the hexagonal pattern offers slightly better signal than the square pattern.

The dependence of SERS on the incident pump power is also investigated for the hexagonal and square lattices at 785 nm wavelength and 633 nm wavelength, respectively. All other parameters were kept identical. The plots of the power dependent Raman signals, in these two cases, are shown in bottom-row of Fig. 5. We found two different regions named as ‘Region-I’ and ‘Region-II’ in both the cases of excitations. The respective regions are observed to be similar except the change in slope which occurs at different power for different excitation pump. The ‘Regions-I’ and ‘Region-II’ clearly show non-proportional (to incident power) SERS intensity. The ‘Region-I’ shows faster rise in SERS intensity while ‘Region-II’ shows a slight trend of saturation.

Power dependent Raman signal with 514 excitation is interesting. For a typical case the signal obtained from square lattice sample is shown in Fig. 7. For a 0.03 mW power the spectrum from the molecules on the flat gold surface

did not reveal any Raman signal, although those from the structured surface showed weak signals of corresponding peaks similar to that obtained for 785 nm and 633 nm laser excitation. The Raman signal was enhanced to a significant level when power increased to 0.3 mW. The peaks are very prominent and well resolved. However, a huge background signal corresponding to fluorescence from R6G molecules is observed in this case.

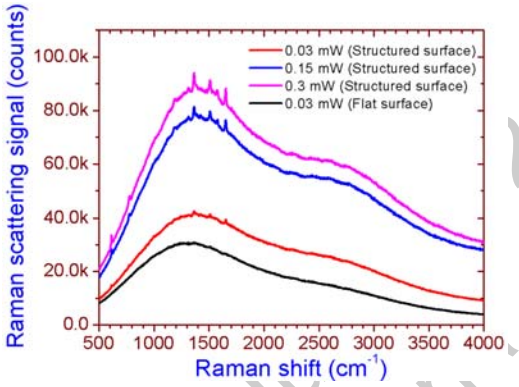

FIG. 6. Raman spectra of R6G+PMMA deposited on plasmonic template of square pattern with periodicity of 800 nm. The pump excitation wavelength is 514 nm laser. The black line represents the sample on flat metal (gold) surface while all other spectra obtained from patterned area.

IV. ELECTROMAGNETIC FIELD SIMULATIONS OF PLASMONIC GRATING TEMPLATES

We now concentrate on the near-field enhancement due to the plasmonic patterning through full 3D simulations using the finite difference time domain method (Optiwave™ package). The large enhancement of the Raman signal is usually due to concentrated electromagnetic near-fields around the metal nanostructures, especially at the metallic edges and corners caused by propagating or localized plasmon resonances or coupled modes of both of them. In order to understand the mechanism, we have modeled the patterned 2D plasmonic templates as having isolated metalized patches on the top, and at the bottom the corresponding continuous metal surface is drilled with holes. Thus, in the cases of square or hexagonal pattern the top metal patches are arranged in a square or hexagonal array, respectively. For simplicity we have considered metal patches as square shaped in both the cases. The structures are very similar to the structures shown in Fig. 1, but with the replacement of circular patches by square patches. The structures are assumed to have a depth modulation of 200nm with a 50:50 duty cycle. Periodic boundary conditions are applied along x and y axes, and anisotropic perfectly matched layers are applied along the growth direction of the structures, i.e. in the z direction. A normally incident plane wave having wavelength of 785nm (unless otherwise stated) is used for the excitation. Polarization of incident pump is set according to symmetry directions. The unit cells for square and hexagonal structures are taken equivalently in real space as shown in Fig. 1. The periodicity of the lattices is fixed at 800 nm.

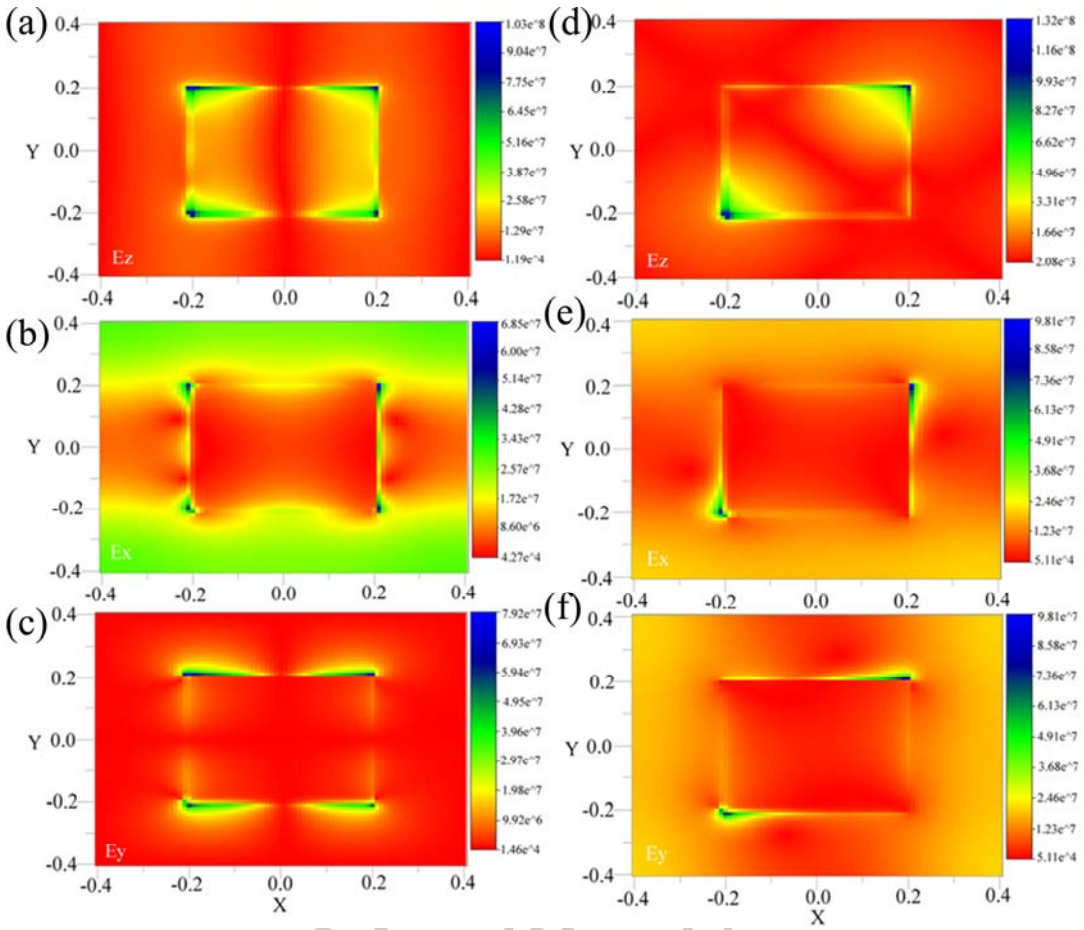

FIG. 7. Surface plots (a-c) of simulated un-normalized electric fields for x-polarized (Γ-X direction) input field of wavelength 785 nm are shown in left-column, whereas the fields distributions for 45^o polarization (Γ-M direction) with respect to X-axis are shown in right-column (d-f). The 2D structure has square arrays with periodicity of 800 nm. The field distributions are as seen on the top of the top-metal patches. E_z field distribution is on the top surface (at top-metal patch) of the structure. X and Y scales are in micron. It can be mentioned here that the Ez simulated field for flat glass substrate is of the order of 10^5 (simulated fields not shown here), indicating the highest Ez field at the corner or edges of the structured templates enhanced by ~10^3. The enhancement in the field at the edges and corners compared to flat portion is also reflected from each figure.

The (E_z, E_x, E_y) field distributions for both the symmetry directions of square periodic structure are shown in Fig. 7. The polarization of input field was set to x-polarization for Γ-X and 45^o polarization for Γ-M directions. For Γ-X symmetry direction the distribution of E_z shows concentrated near-fields around the metal patch edges and corners. The E_x and E_y fields are concentrated along the perpendicular edges of corresponding sides with highest fields at the corners. For Γ-M symmetry direction the E_z near-field distribution shows the highly concentrated fields centred at two opposite corners. The fields are also seen to be weakly confined along the entire edges. E_x and E_y fields show similar near-field localization along the perpendicular edges of the metallic patch. It is observed that the concentration of E_x, E_y and E_z field at the corners for Γ-M symmetry direction is slightly stronger than that for Γ-X symmetry direction. The overall near-fields concentration per unit cell, as reflected from the figures, can slightly be more in the case of Γ-X symmetry direction.

The simulated electromagnetic field distributions (E_z, E_x, E_y) for a 2D hexagonal pattern are shown in Fig. 8. The polarization of the input field was set to X-polarization for the Γ-K direction and 30^0 polarization for Γ-M direction. The left column (a-c) of Fig. 8 represents the (E_z, E_x, E_y) fields for the Γ-K direction whereas, the right column (d-f) represents that for the Γ-M direction. Fields are found to be localized at the edges and corners in a similar fashion as was seen for the square pattern. However, the enhancement of the fields is stronger for the hexagonal pattern than the square pattern. Moreover the interaction of the near fields with the nearest neighbour is clearly observable for the hexagonal pattern (compared field distribution as 'y' subscript an example). This observation shows the evidence for SPR fields at the edges. It can also be seen that the overall field strength per unit cell is higher for the hexagonal pattern than square pattern. Considering the SERS signal dependence on the electromagnetic near-field strength (the

SERS enhancement factor is approximated to be proportional to $(E/E_0)^4$, where E (total field in terms of Ex, Ey and Ez) and E_0 are localized electric near-field and electric field of incident beam, respectively)[8, 17, 21, 27] the hexagonal patterned structures are expected to be superior to the square patterned structures, on an average. We should mention here that the electromagnetic field distribution for rectangular pattern is expected to be similar to the square patterned structure, and hence the simulated results are not presented separately.

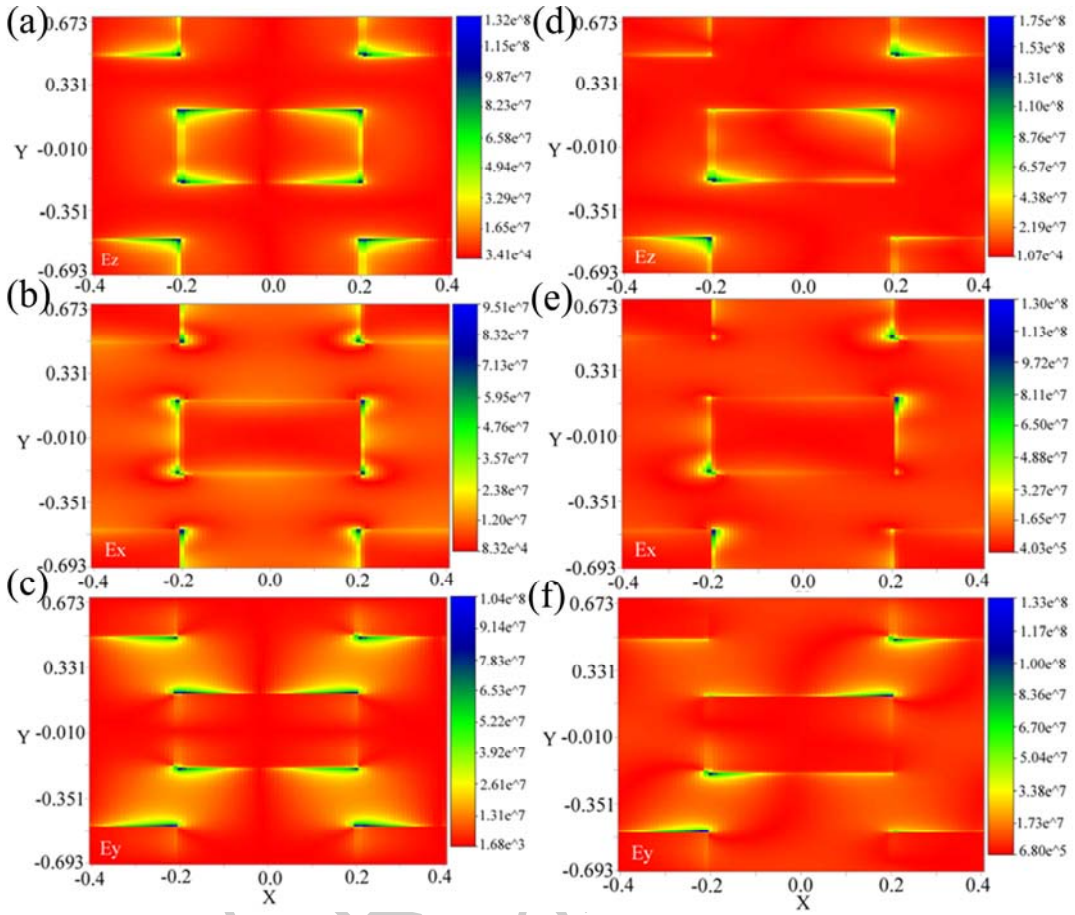

FIG. 8. Surface plots of simulated un-normalized electric field along growth direction (z-axis) for x-polarized (Γ-K direction) input field of wavelength 785 nm are shown in left-column (a-c), whereas the simulated fields for the same structure but with 30^0 polarization (Γ-M direction) with respect to x-axis are shown in right-column (d-f). The 2D structure has hexagonal arrays of square patch with periodicity of 800 nm. E_z field distribution is on the top surface (at top-metal patch) of the structure. X and Y scales are in micron.

To understand the dependence of near-field enhancement on the pump wavelength and its influence on SERS we carried out through 3D simulations of the typical hexagonal pattern with a pump wavelength of 633 nm. This pump wavelength has also been considered for SERS investigation which was presented earlier in section-III (b). In this section, we will show the detailed simulated field distributions across the unit cell of the hexagonal pattern. The field distributions are shown in Fig. 9 below. From the figures it is seen that the field concentration is weak here in comparison to that with 785 nm pump excitation. The coupling of radiation with wavelength 633 nm and the plasmonic pattern with this periodicity at normal incidence is rather weak. Hence the resonance excitation is not strong, which is justified by the measured surface plasmon dispersion data.

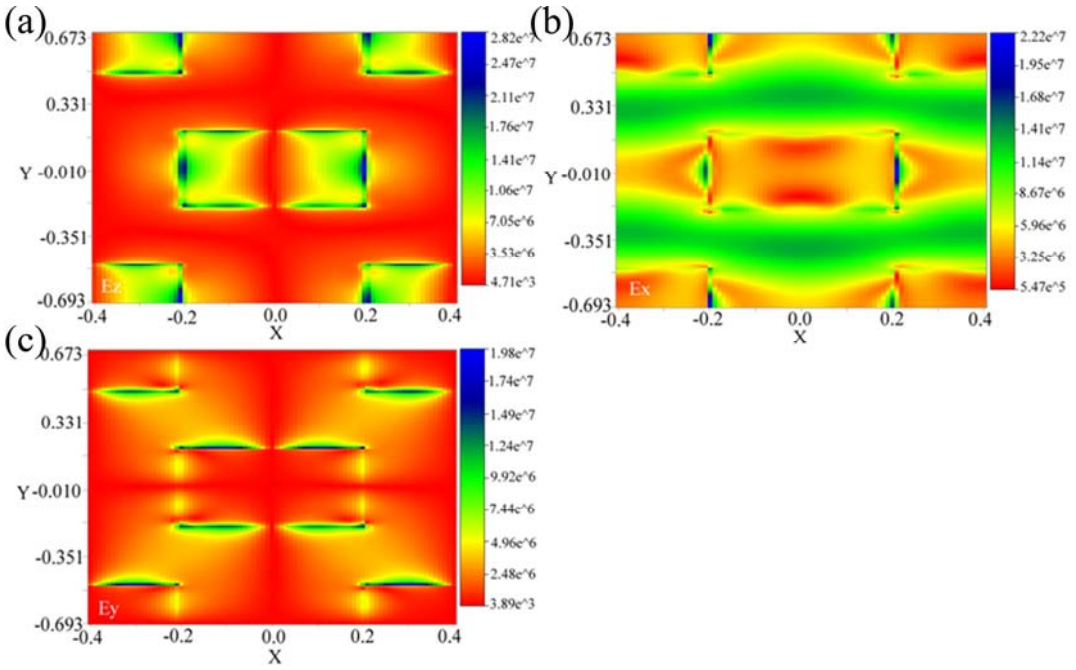

FIG. 9. Surface plots of simulated un-normalized electric fields along growth direction (z-axis) for x-polarized (Γ-K direction) input field of wavelength 633 nm. All other parameters remain same as in the case of 785 nm pump excitation. The distribution of field components are shown in (a), (b) and (b) respectively for Ez, Ex and Ey.

V. DISCUSSIONS AND CONCLUSIONS

Raman scattering data from R6G doped PMMA molecules deposited on plasmonically active 2D gold grating templates having square, hexagonal and rectangular shapes with periodicity of 800 nm have been presented. SPR dispersions for hexagonal as well as square patterns show resonances in the range of 700-900 nm around the 'Γ' point (small angular range, < 10 degree). The observed resonances are very broad in both the cases and spread over certain angle range. As the Raman excitation is focussed through an objective having 50X magnification with numerical aperture of 0.75, and the measurements are performed in air medium, the angular range over which the sample is excited is about 40^o. Similarly the SERS signal is collected back over an angular range of about 40^o. Thus the pump light is very effectively coupled to the surface plasmon resonances over these wavelengths and angular ranges making it highly probable as the mechanism for the strong local fields observed in the simulations and for the enhanced Raman scattering measured from R6G on the plasmonic templates. This strong near-field localization due to surface plasmon resonance enhances the SERS signal to a value of ~ 10^2 (relative to plain gold film) which is of the order of 10^5 compared to the Raman signal from neat solutions since the enhancement on plain gold film is of the order of 10^3.[24] The enhancement factors for the different Raman peaks are different due to the differences in the local density of states (LDOS) (for emitted radiation) of the structured plasmonic templates. Noting that the Raman signals have been obtained from spot of about 5 μm diameter and collected over large angular ranges, the effect of the LDOS variation would be averaged out to a large extent. This is the reason why templates with square or hexagonal patterns show spectra with approximately similar relative peak heights.

The polarization of the incident pump is not so significant as can be concluded from the measured SPR dispersion, which is similar for various orientations for the respective patterns in the desired range of 700 nm to about 900 nm (calculated based on the strongest Stokes shifted Raman peaks in the measured range of up to 1650 cm^{-1} as an example). Therefore from the SPR dispersion point of view the Raman signal should not be drastically different for the square and hexagonal patterns. This observation is supported by the measured Raman data for both the patterns as comparable Raman signals were obtained with the hexagonal geometry proving to be slightly superior to the square one. This slight advantage can stem from the excitation of localized surface plasmon resonances, which although indicated by the simulations, have not been measured in the SPR dispersion measurements. The simulations consistently predict a larger localized near-field for the hexagonal pattern.

A direct consequence of the effective coupling to the SPR through the dispersion is seen when the excitation pump wavelength changed from 785 nm to 633 nm. We note from the measured data in Fig. 3 that no strong SPR excitations are present in the 600-700 nm wavelength range for the square pattern while one can see the presence of broadened SPR dispersion curves in this region for the hexagonal pattern as in Fig. 4. There is clearly a much larger enhancement in the Raman signal for the hexagonal pattern case when the pump wavelength is 633 nm (Fig. 5 c). The

role of the surface plasmons in the SERS becomes apparent here.[8,10,14,15,34,44] We go further down to lower wavelength (514 nm) where plasmonic resonance effect becomes weaker as the absorption by gold dominates. At this wavelength, fluorescence of R6G molecules also dominates and the Raman signal is observed riding over a large background, as presented in Fig. 6. The enhancement in comparison to flat surface is still visible which becomes prominent with higher power.

Power dependent Raman measurements reveal a notable feature that there are two slopes over the applied power range (note that the actual power coupled to sample may be different as has already been mentioned). The change in slopes ('Region-I' and 'Region-II') is observed in both the cases of pump excitations (785 nm and 633 nm laser). In the low power region (Region-I) with the limited data although it is very difficult to say the exact power dependence the high power region (Region-II) shows a linear to near saturation trend. An asymptotic power dependence of SERS signal has been reported previously for thiophenol on Ag island film.[45] It is also generally reported that the Raman signal (Stokes and Anti-Stokes signals) is proportional to incident power[46], although Maher *et al.*[47] reported that the Anti-Stokes signal is quadratic, but Stokes signal is linear to incident power. We note that the near saturation behaviour (non-proportional SERS with incident power) at high power region may arise due to complexities including the degradation of the Raman active molecules and shift of energy to anti-Stokes lines that have not been monitored here, and the change in optical properties of metal nanostructures itself due to local heating by the focused high power laser.

We conclude that large near-fields due to propagating plasmon resonance give rise to the enhanced Raman scattering. A strong correlation between surface plasmon resonance excitation, locally enhanced near-fields and SERS from molecules on structured plasmonic templates has been demonstrated in this communication through different pump excitations and powers, and different patterned plasmonic templates (square and hexagonal patterns). The reproducible SERS templates have been fabricated by simple cost effective laser interference lithography showing potential for applications.

ACKNOWLEDGEMENTS

Asian Office of Aerospace R&D (AFOSR) is thankfully acknowledged for funding via grant no. AOARD–10–4042. The authors also thankful to Dr. S. Mukhopadhyay and Neha Jain at the IISER Mohali, India for assistance in obtaining SERS data.

REFERENCES

[1]M. Fan, G. F. S. Andrade, and A. G. Brolo, Anal. Chimica Acta **693**, 7 (2011).
[2]G. A. Baker, and D. S. Moore, Anal. Bioanal. Chem. **382**, 1751 (2005).
[3]X. –M. Lin, Y. Cui, Y. –H. Xu, B. Ren, and Z. –Q. Tian, Anal. Bioanal. Chem. **394**, 1729 (2009).
[4]X. X. Han, B. Zhao, and Y. Ozaki, Anal. Bioanal. Chem. **394**, 1719 (2009).
[5]B. Sharma, R. R. Frontiera, A. –I. Henry, E. Ringe, and R. P. V. Duyne Mat. Today **15**, 16 (2012).
[6]J. A. Dougan, and K. Faulds, Analyst **137**, 545 (2012).
[7]F. Nagasawa, M. Takase, H. Nabika, and K. Murakoshi, Chem. Comm. **47**, 4514 (2011).
[8]M. Kahl, and E. Voges, Phys. Rev. B **61**, 14078 (2000).
[9]C. S. Rout, A. Kumar, G. Xiong, J. Irudayaraj, and T. S. Fisher, Appl. Phys. Lett. **97**, 133108 (2010).
[10]J. Beermann, S. M. Novikov, K. Leosson, and S. I. Bozhevolnyi, Opt. Exp. **17**, 12698 (2009).
[11]J. P. Schmidt, S. E. Cross, and S. K. Buratto, J. Chem. Phys. **121**, 10657 (2004).
[12]M. Jin, V. Pully, C. Otto, A. van der Berg, and E. T. Carlen, J. Phys. Chem. C **114**, 21953 (2010).
[13]M. D. Doherty, A. Murphy, J. McPhillips, R. J. Pollard, and P. Dawson, J. Phys. Chem. C **114**, 19913 (2010).
[14]J. D. Caldwell, O. Glembocki, F. J. Bezares, N. D. Bassim, R. W. Rendell, M. Feygelson, M. Ukaegbu, R. Kasica, L. Shirey, and C. Hosten, ACS Nano **5**, 4046 (2011).
[15]N. M. B. Perney, F. J. G. de Abajo, J. J. Baumberg, A. Tang, M. C. Netti, M. D. B. Charlton, and M. E. Zoorob, Phys. Rev. B **76**, 035426 (2007).
[16]Y. –C. Liu, C. –C. Yu, and S. –F. Sheu, J. Mat. Chem. **16**, 3546 (2006).
[17]K. D. Alexander, M. J. Hampton, S. Zhang, A. Dhawan, H. Xu, and R. Lopez, J. Raman Spectrosc. **40**, 2171 (2009).
[18]D. –K. Lim, K. –S. Jeon, J. –H. Wwang, H. Kim, S. Kwon, Y. D. Suh, and J. –M. Nam, Nature Nanotechnol. **6**, 452 (2011).
[19]Q. Zhou, Y. Liu, Y. He, Z. Zhang, and Y. Zhao, Appl. Phys. Lett. **97**, 121902 (2010).
[20]L. Gunnarsson, E. J. Bjerneld, H. Xu, S. Petronis, B. Kasemo, and M. Käll, Appl. Phys. Lett. **78**, 802 (2001).
[21]K. D. Alexander, K. Skinner, S. Zhang, H. Wei, and R. Lopez, Nano Lett. **10**, 4488 (2010).
[22]Y. Hou, J. Xu, P. Wang, and D. Yu, Appl. Phys. Lett. **96**, 203107 (2010).
[23]X. Deng, G. B. Braun, S. Liu, P. F. Sciortino, J. B. Koefer, T. Tombler, and M. Moskovits, Nano Lett. **10**, 1780 (2010).
[24]V. Liberman, C. Yilmaz, T. M. Bloomstein, S. Somu, Y. Echegoyen, A. Busnaina, S. G. Cann, K. E. Kron, M. F. Marchant, and M. Rothschild, Adv. Mater. **22**, 4298 (2010).
[25]Y. Jiao, J. D. Ryckman, P. N. Ciesielski, C. A. Escobar, G. K. Jennings, and S. M. Weiss, Nanotechnol. **22**, 295302 (2011).
[26]S. –H. Ciou, Y. –W. Cao, H. –C. Huang, D. –Y. Su, and C. –L. Huang, J. Phys. Chem. C **113**, 9520 (2009).
[27]K. Li, L. Clime, B. Cui, and T. Veres, Nanotechnol. **19**, 145305 (2008).
[28]B. Cui, L. Clime, K. Li, and T. Veres, Nanotechnol. **19**, 145302 (2008).
[29]H. Raether, *Surface Plasmons on Smooth and Rough Surfaces and on Gratings* (Springer-Verlag, Berlin, 1988).
[30]E. Bailo, and V. Deckert, Chem. Soc. Rev. **37**, 921 (2008).
[31]A. P. D. Elfick, A. R. Downes, and R. Mouras, Anal. Bioanal. Chem. **396**, 45 (2010).
[32]J. Henzie, J. Lee, M. H. Lee, W. Hasan, and T. W. Odom, Annu. Rev. Phys. Chem. **60**, 147 (2009).
[33]D. Cialla, R. Siebert, U. Hübner, H. Schneidewind, R. Mattheis, J. Petschulat, A. Tünnermann, T. Pertsch, B. Dietzek, and J. Popp, Anal Bioanal Chem. **394**, 1811 (2009).
[34]A. Kocabas, G. Ertas, S. S. Senlik, and A. Aydinli, Opt. Exp. **16**, 12469 (2008).
[35]P. Mandal, and S. A. Ramakrishna, Opt Lett. **36**, 3705 (2011).
[36]M. R. Gartia, Z. Xu, E. Behymer, H. Nguyen, J. A. Britten, C. Larson, R. Miles, M. Bora, A. S. –P. Chang, T. C. Bond, and G. L. Liu, Nanotechnol. **21**, 395701 (2010).
[37]K. Du, I. Wathuthanthri, W. Mao, W. Xu and C. –H. Choi, Nanotechnol. **22**, 285306 (2011).
[38]C. M. Aikens, and G. C. Schatz, J. Phys. Chem. A **110**, 13317 (2006).

[39]E. J. Zeman and G. C. Schatz, J. Phys. Chem. **91**, (1987) 634.
[40] J. M. Montgomery, A. Imre, U. Welp, V. V. –Vlasko, and S. K. Gray, Opt. Exp. **17**, 8669 (2009).
[41.] http://www.microresist.de/products/room_haas/pdf/ as on 21/4/2012.
[42]S. Astilean, M. Bolboaca, D. Maniu, and T. Iliescu, Romanian Rep. Phys. **56**, 346 (2004).
[43]W. Lin, Appl. Phys. A **102**, 121 (2011).
[44]T. Lopez-Rios, Phys. Rev. B **85**, 125438 (2012).
[45]C. Viets, and W. Hill, J. Phys. Chem. B **105**, 6330 (2001).
[46]T. A. Keif, Ph.D. thesis, University of Southampton, 2006.
[47]R. C. Maher, P. G. Etchegoin, E. C. L. Ru, and L. F. Cohen, J. Phys. Chem. B **110**, 11757 (2006).

Surface enhanced fluorescence and imaging with plasmon near-fields in gold corrugated gratings

P. Mandal*, Prince Gupta, A. Nandi, and S. Anantha Ramakrishna
Department of Physics, Indian Institute of Technology Kanpur, Kanpur-208016, India

Abstract
Surface plasmon near-field assisted fluorescence emission and fluorescence imaging from Rhodamine 6G dye molecules in PMMA (polymethyl methacrylate) thin films deposited on gold coated corrugated gratings have been investigated using blue and green light excitation. The one-dimensional and two-dimensional gold coated corrugated gratings of various periodicities from 400 nm to 1100 nm were fabricated by cost effective laser interference lithography. The fluorescence enhancement depends significantly on the periodicity of the corrugated gratings for the green light excitation centered at 548 nm with maximum enhancement at 500 nm and 1000 nm grating periods. It is observed that a dielectric PMMA spacer layer between the fluorophore layer and the metal surface plays an important role in the enhancement by alleviating quenching and showing a further 3 fold enhancement for a 50 nm spacer layer in comparison to no spacer layer. The dependence of the enhancement with period is caused by the strong coupling of the excitation radiation to the gold gratings resulting in the resonant excitation of propagating surface plasmons. The enhanced near-fields of the surface plasmons assist the excitation of the fluorophores leading to an enhanced fluorescence. Fluorescence imaging shows that the emitted signal is stronger from the 'top' of the structured surface rather than that from the valleys, thereby mimicking the surface structures. Surface plasmon dispersions, measured by angle resolved white light transmission, indicate the strong excitation of surface plasmons resonances over wide angle of excitation by green light for the 500 nm and 1000 nm periods. We show through experiments and computations that enhanced absorption through propagating plasmon resonances is the prime contributor to the enhanced fluorescence.

Keywords: Plasmon near fields, fluorescence of R6G, laser interference lithography, fluorescence imaging

*Corresponding author's Tel: 91 512 259 6601
Fax: 91 512 259 0914
Email: prasanta75@gmail.com

1 Introduction

Surface enhanced fluorescence (SEF) or metal enhanced fluorescence (MEF) is a process in which the fluorescence from molecules placed in the vicinity of metallic structure is highly enhanced by the strong interaction between electromagnetic near-fields and molecules, and due to the modification of the radiative decay rates. SEF/MEF has commonly been used for bio-molecular fluorescence imaging/mapping, especially for bio-medical applications.[1-3] Strong localized electromagnetic fields at the vicinity of metal nanostructures or between two metal nano-objects separated by small gap (a few nanometers) due to plasmonic excitation can resonantly interact with nearby fluorophores and modify the fluorescence decay rate (increase or decrease), resulting in enhanced or decreased fluorescence, respectively.[4-10] This enhancement or quenching has been observed for a variety of material systems[11-16] and also depends upon the separation between the metallic surface and the fluorophores, which can usually be manipulated as per requirements by using dielectric spacer layer.[4,9,17-19]

It is well known that nanostructures made of plasmonic materials like gold and silver can resonantly interact with radiation over a range of wavelengths from micro-scale to nano-scale through the excitation of surface plasmon resonances.[20] These resonant interactions can result in the generation of highly enhanced and localized fields in the close vicinity of the nanostructures as well as provide for a potent manner of changing the local electromagnetic environment. The interaction of a molecule in the vicinity of these plasmonic structures, with radiation can be drastically modified by these effects. Surface enhanced Raman scattering (SERS) has been a very popular application that utilizes the large local field enhancement.[21,22] Structured plasmonic materials are also very promising for enhancing the fluorescence from molecules via the highly concentrated near-fields and drastically modified photonic density of modes.[13-14,23-24] Specially designed nano-antenna structures such as bowtie nano-antennas have been studied and a fluorescence enhancement of ~ 10^3 is reported.[25,26] Furthermore, metal nano-tips have also been employed to realize enhanced fluorescence with an optimized separation between tip and the fluorophores that can easily be controlled.[27-29] The strong influence of the local electromagnetic near-fields and their manipulation through the structuring, the type of fluorophore, the dielectric environment, the separation between the fluorophores and metal structures, and the type of metal used are important aspects to determine the fluorescence enhancements. Hence periodic nano-patterned plasmonic templates with different geometries are promising for

SEF application in view of the reproducibility that they offer. Further, due to the periodic structure, interesting interplay of Bragg scattering and the plasmonic effects can also be seen. Detailed knowledge of the plasmonic characteristics, surface plasmon dispersion and photon density of modes for these systems can result in the purposeful design of optimized structured plasmonic templates for SEF application at specific excitation wavelengths.

In this communication, we present the surface enhanced fluorescence from R6G molecules placed in a simple plasmonic system, viz, corrugated gold gratings made using the highly cost effective technique of laser interference lithography. Due to the plasmonic coupling and consequent the large localized fields, highly enhanced fluorescence with upto 60 times enhancements are seen for efficient excitation with green radiation, while blue light excitation is not effective due to the absorption in gold. The fluorescence enhancement is shown to depend highly on the period of the gratings, and the detailed correlation to the underlying plasmonic assisted excitation of the molecules is shown by experimental measurements of the surface plasmon dispersions, fluorescence images of the gratings, and detailed numerical simulations of the gratings that show large localized electromagnetic fields for certain periodicities.

The paper is structured into the following sections. The details of the fabrication of the gratings and experimental methods are given in Section-2. Section-3 discusses the fluorescence measurements and the imaging, while the measurement of surface plasmon dispersion is discussed in Section-4. The numerical simulations carried out using the Optiwave-^{TM} software package based on the Finite Difference Time Domain (FDTD) method are discussed in Section-5. After detailed discussions, we present our conclusions in Section-6.

2 Experimental details

Fabrication of plasmonic corrugated gratings was performed by the following steps: Positive-tone photoresist (ma-P 1205 from Micro-resist technology, Germany) was spin coated at 3000 rpm for 45 seconds on cleaned glass plates, and subsequently baked at 80 °C for 1 minute. The photoresist coated glass plates were then exposed to two-beam laser interference patterns produced by a diode pumped solid state laser (DPSSL) having wavelength of 473 nm, typically for 20 minutes. While continuous 20 minutes exposure was used to generate one-dimensional (1D) periodic nano-grating templates, double exposures (10 minutes each) methodology was adapted for the generation of two-dimensional (2D) periodic nano-grating templates. A sample stage rotation of 90^o or 60^o was performed between the first and the second exposure to generate square or hexagonal patterns, respectively. The period for the 1D gratings (primarily used for this study) was in the range of 400 nm to 1100 nm in accordance with the relation $p=\lambda/\sin\theta$, where p is the period of the structure, λ is the wavelength of the laser used to produce the interference and θ is the half angle between the two interfering beams. The development of the exposed photoresist films in a standard developer resulted in periodically patterned photoresist films on the glass substrates. A thin layer (40 nm, unless otherwise stated) of gold was thermally evaporated onto the top of the patterns. A schematic of the laser interference lithography (LIL) set up along with typical expected 1D and 2D patterns which can be generated using this set up are shown in Fig. 1 for easy understanding.

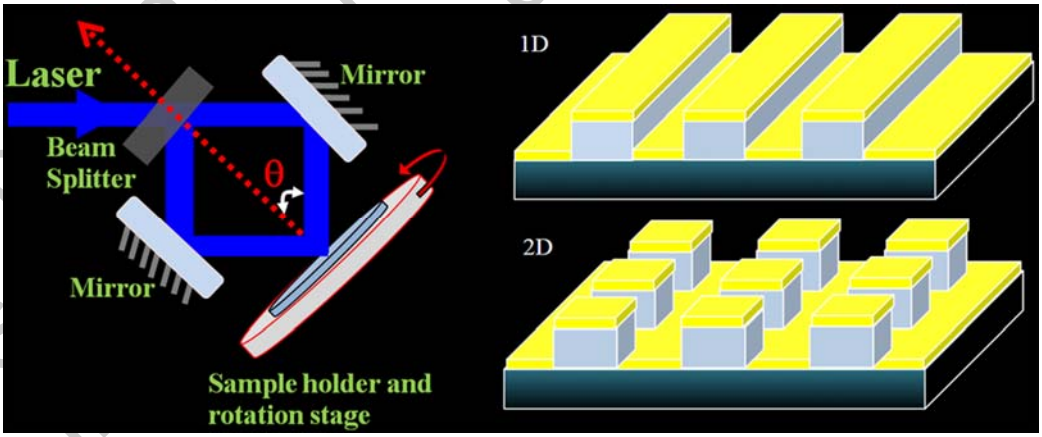

Fig. 1 Schematic diagram illustrating the laser interference lithography (LIL) set up, and the typical 1D and 2D patterns that can be generated using this set up are shown in the left-panel and right-panel, respectively. The yellow colour in the 1D and 2D patterns represents the evaporated gold on the LIL generated gratings.

Fluorescent molecules Rhodamin-6G were mixed in PMMA (PMMA in chlorobenzene purchased commercially from MICROCHEM, Germany) and the homogeneous solution with a concentration of R6G in

PMMA of 26 μmol was spin coated on the plasmonic gratings, which resulted in approximately 25 nm film thickness. For reference purposes, the same solution was also spin coated onto flat gold coated glass substrates. The excitation of the fluorophores was performed with two Hg bands (λ_{blue} = 488 nm with FWHM 23 nm, and λ_{green} = 548 nm with FWHM 5 nm) using an Olympus BX51 fluorescence microscope through 100X objective. The fluorescence intensity was collected through the same objective in the reflection mode and coupled to an Ocean Optics HR2000+ Spectrometer having a resolution of 0.5 nm through an optical fibre. Fluorescence images of the plasmonic samples were obtained using a CCD camera.

The surface plasmon dispersion on the gratings was studied through angle dependent broad band (450 nm to 1000 nm) transmission measurements in the angular range of -40^0 to $+40^0$ with a step of 0.2^0. The white light source was a 100 watt tungsten-halogen lamp with a final collimated beam width of ~1 mm. A polarizer was used to illuminate the gratings with transverse magnetic (TM) polarization mode of input beam to match sample orientation. An Ocean Optics spectrometer (model: HR2000+) was used to spectrally analyze the transmitted beam.

3 Experimental results

3.1 Fluorescence imaging

Fluorescence images of the R6G in PMMA coated onto corrugated gratings with variety of lattice structures are shown in Fig. 2. We show the white light transmission image of a 1D grating with 1000 nm period in Fig. 2a and that of a 2D square grating with 1000 nm period in Fig. 2d. Fluorescence images of the 1D and 2D gratings when excited with green light and

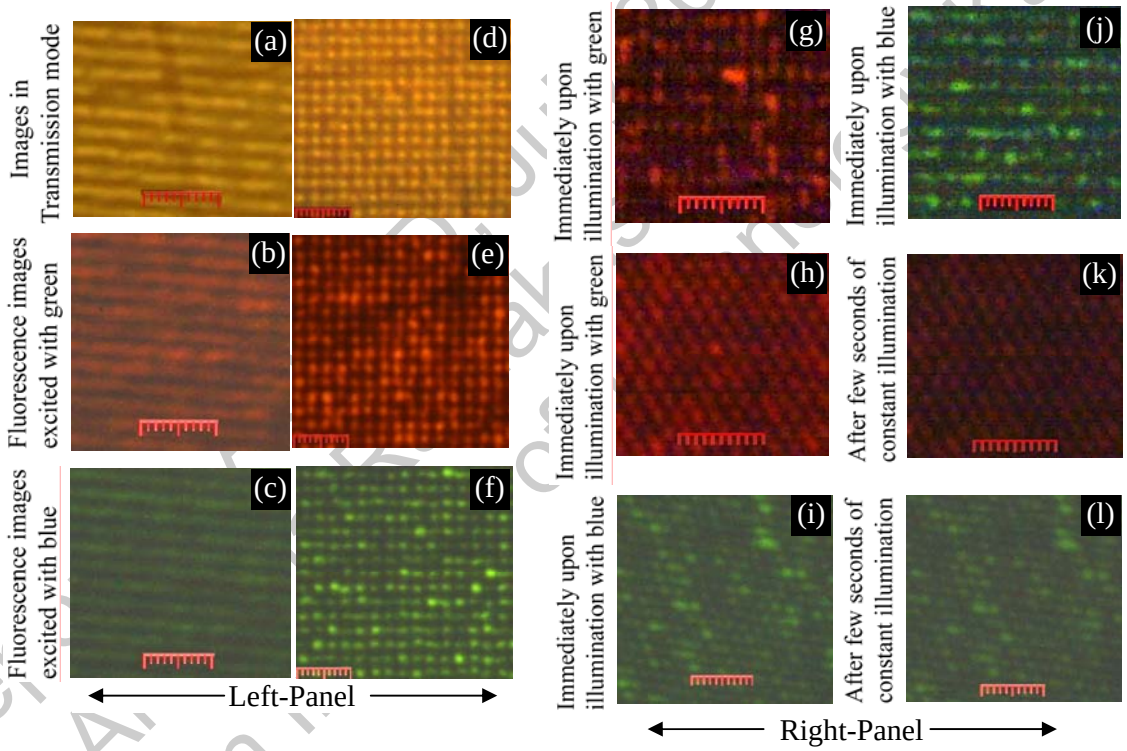

Fig. 2 Fluorescence images of few typical samples after the green and blue excitations. Red coloured fluorescence images are obtained with green excitation while dark greenish coloured fluorescence images are for blue excitation. Yellow coloured images are obtained in the transmission mode. Images are obtained on 1D gold corrugated gratings with periodicity of 1000 nm (a-c), 2D gold corrugated gratings with periodicity of 1000 nm (d-f). Images (g, j) correspond to a rectangular grating with side arms of 800 nm and 1300 nm. Images (h, k, i, l) correspond to a hexagon with periodicity of 800 nm. Images (h, i) are obtained just after the excitation while (k, l) after few seconds.

blue light are shown in Fig. 2b and Fig. 2c, and Fig. 2e and Fig. 2f, respectively. It is clear that the fluorescence emission from the molecules is spatially inhomogeneous, although the distribution of R6G molecules is reasonably uniform over the entire surface.[30] The Figs. also show that fluorescence image has same symmetry as the underlying structures. This feature is common to gratings with hexagonal and rectangular symmetries shown in Fig. 2g to Fig. 2l. The spatial inhomogeneous emission is due to spatially inhomogeneous excitation due to the plasmonic near-field of the grating, an aspect that will be discussed in detail later.

It was noted that the fluorescence intensity typically reduces drastically in time over a few seconds immediately after the excitation radiation was switched on.[6] This occurs due to the accumulation of R6G molecules in non-radiative triplet states.[31] The typical triplet life-time of dye molecules in solid state host medium is in the range of 10 ms to 100 ms.

3.2 Fluorescence measurements

Fluorescence spectra of R6G dye doped PMMA films coated on to 1D corrugated gratings having different periods (400 nm to 1100 nm) are measured for green and blue excitation light. For green excitation, the spectral shapes from all the gratings are observed to be similar in nature. Similarly, the spectra obtained with blue excitation are also similar for all the gratings, although they are necessarily different from the ones for green excitation. The primary difference is the total fluorescence intensity obtained for the different grating periods. In Fig. 3a, we show the fluorescence spectrum obtained from R6G in PMMA on corrugated grating having a period of 900 nm along with the corresponding reference spectrum obtained from plain gold coated substrate, for green excitation. Both the sample spectrum and the reference spectrum show a sharp cut-off for wavelength below 590 nm due to transmittance of the filter used. It is observed that the fluorescence signal is enhanced by about 5 times compared to the reference signal. In the normalized spectra (normalized with respect to the intensity at 600 nm) shown in Fig. 3b, it is observed that the spectral width of the fluorescence from the corrugated grating is slightly more in comparison to the reference spectral width due to the inhomogeneous broadening caused by the inhomogeneous electromagnetic environment felt by the molecules. For blue excitation, a similar trend is noticed (Figs. c and d). However, the fluorescence signal from the structured region is only about 2 times larger compared to the reference signal in this case.

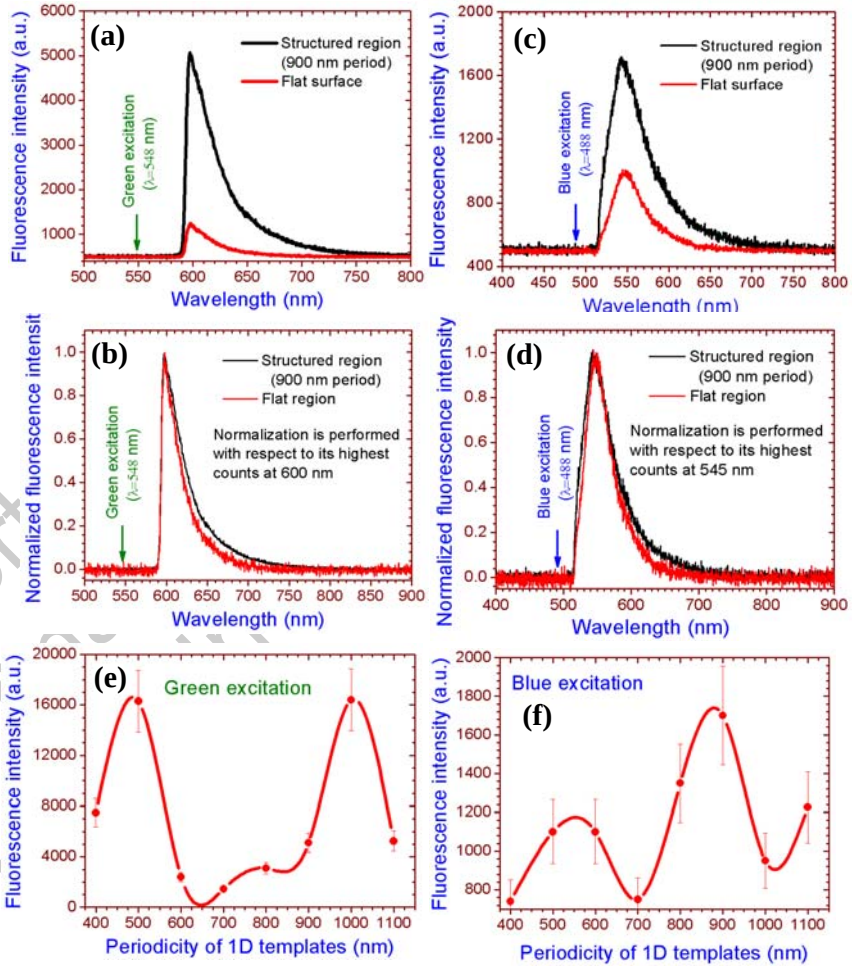

Fig. 3 Typical fluorescence spectra of 1D sample having 900 nm period after excitation with green (a) and blue (c). The spectra from the flat gold coated surface for corresponding excitations are also shown for comparison. The corresponding normalized spectrum is shown in the respective Fig. 3b and Fig. 3d. The periodicity dependent intensity profiles for green and blue

excitations are shown in Fig. 3e and Fig. f, respectively. The profiles are obtained for 600 nm peak and 545 nm peak in the case of green and blue excitations, respectively.

We will now discuss about the period dependence of the fluorescence intensity for green as well as blue excitations. The detailed dependence of the fluorescence enhancement with the period of the corrugated gratings is shown in Fig. 3e and Fig. 3f for green and blue excitations, respectively. The dependence in Fig. 3e for green excitation shows a systematic variation in intensity, showing the strongest signals at 500 nm period and 1000 nm period. The fluorescence signal is comparably large at these two periods. It is also observed that the enhancement for these two periods is about 15 times compared to the corresponding reference signals. It is interesting that instead of single optimized period the enhancement is modulated with the period. For the blue excitation, however, the enhancements are much smaller and comparable to each other having no such clear systematic dependence.

It is mentioned earlier that the spacer layer between fluorophore and metal surface plays a crucial role for the enhancement of fluorescence. We have also checked this issue by using the optimized 1000 nm periodic structure. On the structured surface, we first put a PMMA (dielectric) spacer layer of various thicknesses and subsequently we put the R6G doped PMMA layer. Figure 4 shows the fluorescence peak intensities for green excitation with various spacer layer thicknesses. All other parameters are kept identical. It is to be mentioned that before putting R6G solution, the PMMA spacer layer coated templates were heated to 100 °C for 1 minute to remove any moisture and make it uniform. The dependence shows an optimum layer thickness between 50 to 100 nm giving the highest fluorescence signal, after which it falls again with increasing spacer thickness. It is observed that below 25 nm spacer layer thickness the fluorescence intensity is almost comparable to that without the spacer layer. The highest signal obtained with the optimized spacer layer thickness is nearly 4 times as high as the signal for no spacer layer.

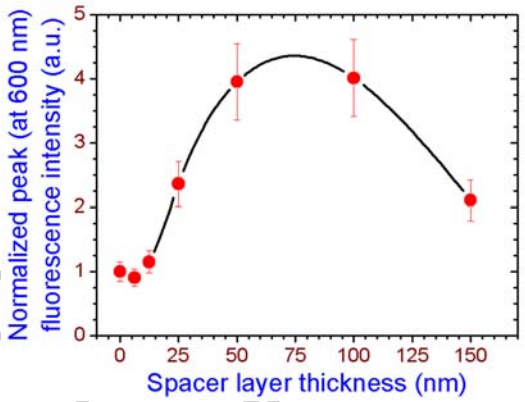

Fig. 4 Peak fluorescence intensity from R6G on 1D sample having 1000 nm period for green light excitation with respect to spacer layer thickness. The peak is normalization with the fluorescence peak counts obtained for sample with 1000 nm period and no spacer layer. The solid line is a guide to the eyes only.

We checked the photo-stability of the fluorophore under continuous pump excitation. The fluorescence spectra obtained for a sample of 900 nm period for green as well as blue excitations under continuous excitation are shown in Fig. 5. The intensity falls with time for both the excitations, although in the case of green excitation the fall is more rapid. This has already been mentioned during the study of fluorescence images that the images became darker and darker within few tens of seconds of exposure due to accumulation of molecules in the non-radiative triplet states. Inset in the respective figure shows the plot of the peak intensity at 600 nm for green and 545 nm for blue excitation against various times of continuous exposure (in seconds). The intensity fall follows an exponential decay fit showing half life of the order of 50 seconds for green excitation, whereas for blue excitation the half life is longer. Similar observations have been reported previously by Gryczynski *et al*.[6] on Rhodamine dye, who also showed that it can be overcome by the introduction of inorganic quantum dots which are highly photo-stable.

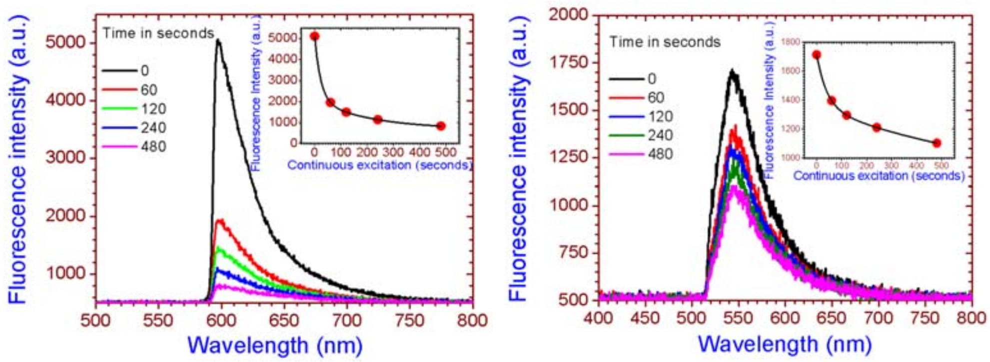

Fig. 5 Fluorescence spectra of R6G on 1D corrugated grating having 900 nm period after excitation with green (left) and blue light (right). The spectra were recorded after various time interval as mentioned in the legend. The fall of the peak intensity (evaluated for 600 nm for green and 550 nm for blue) versus time of continuous excitation is shown in the inset.

4 Surface plasmon dispersion

The dispersion of surface plasmons (SP) on the corrugated gratings are important in understanding the role of plasmon resonance excitation and coupling of pump light with the molecules, and hence the SEF. The change in the density of photonic modes mediated by SP can also play a role in SEF. The wavelength of light 'λ_{res}' to excite plasmon modes associated with the gratings can be correlated with the conservation of in-plane momentum by the following rule:

$$\lambda_{res} = \frac{p}{m}.[\sqrt{\frac{\varepsilon_m.\varepsilon_d}{\varepsilon_m + \varepsilon_d}} - \sin\theta] \qquad (1)$$

where, the symbols p, m, ε_m, ε_d and θ refer to period of the 1D gratings, order of diffraction, relative permittivity of metal, relative permittivity of dielectric and angle of incidence, respectively. Drude dispersive model has been adapted for gold (Au) with plasma frequency (ω_p) of 1.37×10^{16} rad/s and collision frequency (ν) of 1.076×10^{14} rad/s.[32] The dielectric constants for photoresist and PMMA were taken as 2.62[33] and 2.25,[34] respectively.

Experimentally measured dispersions and theoretical plots using equation-1 are shown in Fig. 6. The SPP modes can be identified with the corresponding theoretical plots on a one-one basis. Surface plasmon dispersion for the 400 nm 1D structure is observed only in the wavelength range of 600 nm-850 nm with the m = ±1 order. The higher order modes m = ±2 are not visible due to the intrinsic absorption in the gold below 500 nm. Likewise, from the SPP resonance dispersion for 500 nm period, it can be observed that the resonance dispersions of the PMMA-metal interface as well as photoresist-metal interface co-exist (m= ±1 order), and the PMMA-metal resonance extends towards the lower wavelengths until about 550 nm. The existence of this resonance around 550 nm is important for the excitation of surface plasmons at this wavelength and will be discussed in detail later. The higher order modes (m=±2) also exist, but are relatively weaker and broad. The angular spread of the resonance for the various modes will boost the resonance excitation of the plasmon during fluorescence excitation with large numerical aperture objective. For the structure with a period of 700 nm, the higher order modes with m = ±2 are spread over the wavelength range of 550 nm to 800 nm. However, the resonance mode is weak beyond 600 nm. The angular spread is also within small values of incidence angle compared to the 500 nm period structure. The m= ±1 modes are hardly seen in the longer wavelength side at higher incidence angles (> 10^0). These observations suggest the possibility of only weak coupling of the green pump (say 548 nm) to the structure. In contrast, the structure with 1000 nm period shows similar resonance features as seen in the case of the 500 nm periodic structure. The 1100 nm periodic structure shows weak and narrow higher order modes (m=±2, ±3) within the angular range of ± 60^0. The existence of the surface plasmon resonances (SPR) for the corrugated gratings clearly indicates the possibility of strong excitation of SPR by the pump input of 548 nm green line.

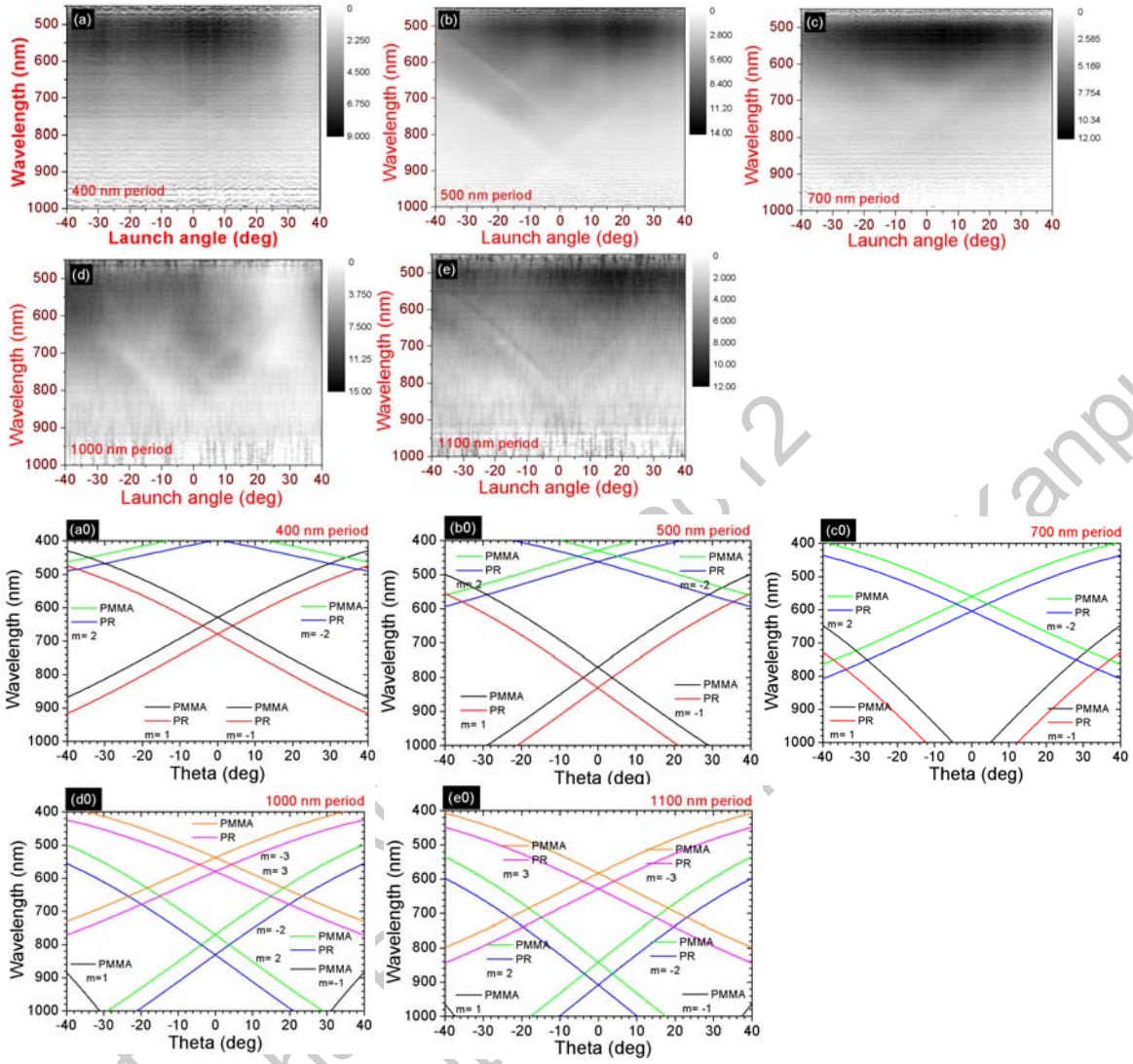

Fig. 6 Experimentally measured SPP dispersion plots (a-e) and it's corresponding theoretical plots (a0-e0) (using analytical formula as in equation-1) for 1D plasmonic templates are shown in the form of surface plots. The dispersions reveal the SPP modes change its excitation resonance wavelength with launch angle and have good correspondence with theoretical plots.

5 Electromagnetic fields simulation of plasmonic nano-gratings templates

The enhanced fluorescence and the systematic change in the enhancement for specific periodic structures is caused by the huge near-field enhancement at the metal edges and corners through the resonant excitation of surface plasmons. To unveil the mechanism, we carried out electromagnetic field simulations for these plasmonic gratings using the Optiwave™ software based on FDTD method. The grating period was systematically varied from 400 nm to 1100 nm. The gratings have typically a modulation depth of about 200 nm with a 50:50 duty cycle, and most of the gold patches are located at the top and bottom of the corrugated grating. For simplicity, we consider that the metal surfaces (at the top and bottom) are isolated, although there is a thin gold layer on the side walls due to the evaporation process. Since the modulated enhancement is most significant for the green excitation centred at 548 nm. We use TM polarized plane wave at normal incidence having a wavelength of 548 nm for the entire simulation. A unit cell with periodic boundary conditions along Z-axis is assumed, while anisotropic perfectly matched layers are applied along the growth direction of the structures, i.e., in the X direction. The interaction of pump light with the local dielectric and metal objects produces the scattered, localized electromagnetic near-fields whose electric field components (E_x and E_z) are primarily the major contributors for the SEF. Although the combined E_x and E_z

fields are effective, the E_x fields seem to be the dominating contributor to SEF, and hence in Fig. 7 we have presented only the distribution of E_x component.

Distributions for simulated E_x near-field component for all the 1D periodic structures are shown in Fig. 7. It is observed that for all the unit cells of different periods, the E_x field is strongly localized in both the 'top-ridges' as well as in the 'bottom-valleys'. However, the field strength is comparatively stronger at the 'top' surface rather than inside the 'valleys'. Moreover in some cases the field is extremely strong and spread over larger areas on the top-ridges. We now discuss the field distribution sequentially starting with the 1100 nm periodic structure. For this structure, the field is weakly localized in the valleys, the edges and corners, and at the top-ridges. For 1000 nm periodic grating, the E_x field is now localized with larger spread at the top-ridges and valleys. It is clearly seen that the field is much stronger compared to 1100 nm periodic structure. It should also be noted that the overall field

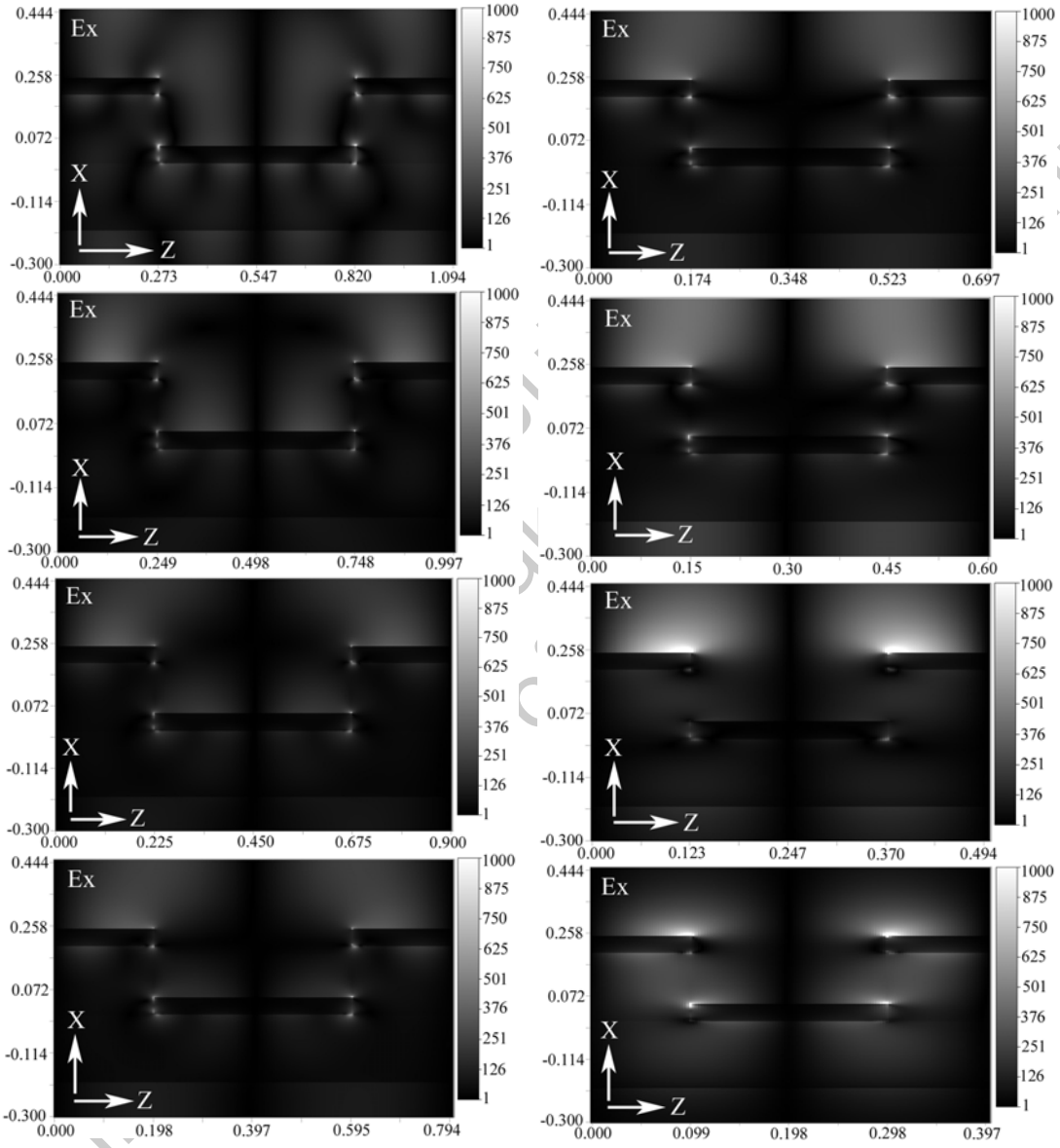

Fig. 7 Simulated electromagnetic near-field (E_x) distribution with the unit cell for various 1D periodic gratings (periods varying from 400 nm to 1100 nm). The value of the periodicity is reflected from the 'Z' value along the horizontal scale with each of the figure.

strength per unit cell is stronger for 1000 nm periodic structure. The E_x near-field for 900 nm, 800 nm and 700 nm periodic structures are almost similar with a trend that, with the decreasing periodicity, the field becomes stronger at the top-ridges and weaker at the valleys. For the grating with 600 nm period the top-ridges becomes much stronger

with almost no field at the valleys. For 500 nm periodic structure the field is extremely high at the top-ridges with wider spread but with almost no field inside the valley. Grating with 400 nm period shows the fields at the 'top' as well as at the 'well' and seems they are coupled through the part of the resist layer. The overall field useful for the fluorescence excitation is seen to be the highest in the 500 nm and 1000 nm periodic structures compared to other periodic structures. Thus, from the simulation studies one expects larger enhancement of the electromagnetic near-field for some specific structures (here 1000 nm and 500 nm periodic structures) due to strong coupling of the pump input to the structure. As the near-field boosts the excitation of the fluorophores, we expect relatively larger enhancement for these specific periodic structures.

6 Discussions and conclusions

We have studied surface plasmon assisted fluorescence enhancement from R6G doped PMMA films coated on plasmonic corrugated gratings. Two different pump wavelengths for the excitation of fluorophore on plasmonic gratings were also considered to understand the effect of the excitation mechanisms. We observed a systematic dependence of fluorescence enhancement on the grating periodicity in the case of green excitation having wavelength band centred at 548 nm compared to the blue excitation centred at 488 nm. In general, there are two processes by which the fluorescence can be enhanced: one, by more efficient excitation that can be caused by enhanced fields of the excitation radiation; and two, by a modification of the photonic density of modes due to a modification in the electromagnetic surroundings of the molecules. Plasmonic structures can easily enhance the fields of the excitation radiation via the enhanced localized fields of the surface plasmon excitation. They can also enhance the photonic LDOS (local density of states) as in the case of nano-antennas,[25] in which case, the radiative transitions can be strongly enhanced over the non-radiative processes in the molecules. This engineering of the molecular decay rate has also been very popular in the literature.[16] In our case, the fact that there is strong dependence on the grating periods for the green excitation compared to the blue excitation; as well as, the large modulation for the green light indicates that it is the plasmonic processes that give rise to the enhanced absorption/excitation. The computer simulations indicate very strong plasmonic excitation for gratings with periods of 500 nm and 1000 nm, which is in close correspondence with the experimental observation of large fluorescence enhancements in gratings with these periods. The measured surface plasmon dispersions also show the presence of the surface plasmon in these gratings with a large angular spread which favors the excitation of the SPs (surface plasmons) by the large numerical aperture of 0.9 in the 100X objective used for study. Thus, we can effectively conclude that strong plasmonic coupling and consequent enhanced absorption of the pump radiation is responsible for the enhanced fluorescence with green light excitation. These effects are hardly felt for excitation with the blue light because of the strong absorption of the exciting radiation in gold due to inter band transitions.

As the R6G molecule already has an enormous quantum efficiency (>90%) for the fluorescence in most of the host materials,[31] large enhancements in the fluorescence are not possible by increasing the radiative transition probabilities over the non-radiative transitions. However the de-excitation of the molecules by coupling to non-radiative plasmon modes is still a possibility. In fact, this manifests in the strong quenching of fluorescence of molecules that are very close to the metallic film. It is well known that a dipole induces an oppositely oriented image dipole in perfectly conducting film. Thus, a dipole placed on a PEC (perfect electrical conductor) cannot radiate efficiently. This manifests for molecules placed directly on the gold film, which although not a perfect conductor at optical frequency, strongly quenched the emission from the molecule. The molecule is enable to radiate while the strong near-fields of the molecule couple to the non-radiative plasmonic excitation, thereby de-exciting the molecules. When the molecules are, however, placed some distance away from the gold film, the emissions from the molecules and their respective images do not destructively interfere to cancel out each other and the plasmonic enhancement to the excitation results in the strong fluorescence enhancement. Placing the molecules too far away from the surface reduces the plasmonic enhancement effect due to the rapid decay of the near field of the SPs with distance from the grating surface. This explains the optical distance (spacer layer thickness) of about 50 nm to 100 nm from the grating, when the fluorescence enhancement is most effective and largest.

To further understand whether the radiative processes are indeed enhanced in comparison to non-radiative processes, we carried out some preliminary studies on lifetime measurement on the fluorescence from these gratings. These studies, while not complete, indicate that there can be about 20% change in the radiative life time of this R6G molecule. Thus, while the corrugated gratings modulate the fluorescence emission via modified photonic LDOS, the large fluorescence enhancement for high quantum efficient molecules such as R6G is predominantly due to efficient excitation of the molecule by enhanced surface plasmon near-fields.

Finally as can be seen from the simulated data (Fig. 7), the near-field is mostly confined to the regions at the edges and corners, and spread over certain areas of the top-ridge surface of the metallic patches. The plasmonic interaction with fluorophores in these regions will be much stronger and the strong excitation by the pump beam is expected to increase the fluorescence. Thus, fluorophores residing on the top of the structured surface feel stronger near-fields resulting in high emission compared to surrounding area. This can be seen from the fluorescence images

(in Fig. 2) that mimic the geometrical structures of the original gratings. The darkening of the fluorescence images and more rapid fall in the fluorescence due to accumulation in the triplet states for the green excitation compared to the blue excitation is due to the strong near-field excitation. The more efficient excitation not only boosts the fluorescence but also causes more rapid accumulation of the molecules in the triplet states. As has been noted before, the excitation of surface plasmon resonances is very weak for the blue light excitation, and hence the dependence on the grating period is weak.

In conclusion, we have studied surface plasmon enhanced fluorescence and fluorescence imaging from Rhodamine 6G doped PMMA coated on plasmonic corrugated gratings. The gratings were fabricated by cost effective laser interference lithography and metal vapor deposition. The enhanced fluorescence signal for the molecules on 1D gratings strongly depends on the periodicity of the gratings and the pump wavelengths. The modulated enhancement of the fluorescence signal with green excitation light is due to the resonant excitation of propagating surface plasmon and strong coupling of the pump light to the molecules, resulting in enhanced absorption and excitation of R6G molecules. Rapid decrease in the fluorescence over few tens of seconds is due to the transfer of molecules to the non-radiative triplet states. The fluorescence images support the idea of efficient excitation of the molecules only in some regions as they mimic the geometrical structures of the gratings. By using a molecule like R6G with high quantum efficiency, it has been possible to study the plasmonic effects on enhanced excitation of the molecules, while not being affected extremely by the effects of modified photonic LDOS and the consequent changes in the radiative efficiencies.

ACKNOWLEDGEMENTS

Asian Office of Aerospace R&D (AFOSR) is thankfully acknowledged for funding via grant no. AOARD–114047.

References

1. E. Fort, and S. Grésillon, J. Phys. D: Appl. Phys. **41** 013001 (2008).
2. X. Cui, K. Tawa, H. Hori, and J. Nishii, Adv. Funct. Mater. **20** 546 (2010).
3. Joseph R. Lakowicz, Plasmonics **1** 5 (2006).
4. W. Zhang, F. Ding, W. –D. Li, Y. Wang, J. Hu, and S. Y. Chou, Nanotechnol. **23** 225301 (2012).
5. K. Ray, R. Badugu, and J. R. Lakowicz, J. Am. Chem. Soc. **128** 8998 (2006)
6. I. Gryczynski, J. Malicka, W. Jiang, H. Fischer, W. C. W. Chan, Z. Gryczynski, W. Grudzinski, and J. R. Lakowicz, J. Phys. Chem. B, **109** 1088 (2005).
7. J. –H. Song, T. Atay, S. Shi, H. Urabe, and A. V. Nurmikko, Nano Lett. **5** 1557 (2005).
8. L. Ma, and W. Chen, J. Appl. Phys. **107** 123513 (2010).
9. I. M. Soganci, S. Nizamoglu, E. Mutlugun, O. Akin, and H. V. Demir, Opt. Exp. **15** 14289 (2007).
10. T. Ozel, I. M. Soganci, S. Nizamodlu, I. O. Huyal, E. Mutlugun, S. Sapra, N. Gaponik, A. Eychmüller, and H. V. Demir, New. J. Phys. **10** 083035 (2008).
11. P. Petrou, I. Raptis, S. Kakabakos, T. Speliotis, A. Gerardino, and N. Papanikolaou, Microelectron. Engg. **88** 1845 (2011).
12. P. Mandal, A. Singh, S. Kasture, A. V. Gopal, and A. S. Vengurlekar, "Plasmon assisted intense blue–green emission from ZnO/ZnS nanocrystallites", *Opt. Mater.* **33** (11), 1786-1791 (2011), http://dx.doi.org/10.1016/j.optmat.2011.06.011.
13. Y. –H. Chan, J. Chen, S. E. Wark, S. L. Skiles, D. H. Son, and J. D. Batteas, "Using Patterned Arrays of Metal Nanoparticles to Probe Plasmon Enhanced Luminescence of CdSe Quantum Dots", *ACS Nano* **3** (7), 1735-1744 (2009), http://pubs.acs.org/doi/full/10.1021/nn900317n.
14. E. Hwang, I. I. Smolyaninov, and C. C. Davis, "Surface Plasmon Polariton Enhanced Fluorescence from Quantum Dots on Nanostructured Metal Surfaces", *Nano Lett.* **10** (3), 813-820 (2010), http://pubs.acs.org/doi/full/10.1021/nl9031692.
15. S. Kühn, U. Håkanson, L. Rogobete, and V. Sandoghdar, "Enhancement of Single-Molecule Fluorescence Using a Gold Nanoparticle as an Optical Nanoantenna", *Phys. Rev. Lett.* **97** (1), 017402 (2006), http://link.aps.org/doi/10.1103/PhysRevLett.97.017402.
16. Joseph R. Lakowicz, *'Principles of Fluorescence Spectroscopy', (p841-p871),* Springer, 2006.
17. K. A. Kang, J. Wang, J. B. Jasinski, and S. Achilefu, "Fluorescence Manipulation by Gold Nanoparticles: From Complete Quenching to Extensive Enhancement", *J. Nanobiotechnol.* **9**, 16 (2011), http://www.jnanobiotechnology.com/content/9/1/16.
18. P. Anger, P. Bharadwaj, and L. Novotny, "Enhancement and Quenching of Single-Molecule Fluorescence", *Phys. Rev. Lett.* **96** (11), 113002 (2006), http://link.aps.org/doi/10.1103/PhysRevLett.96.113002.
19. Y. Zhang, A. Dragan, and C. D. Geddes, "Wavelength Dependence of Metal-Enhanced Fluorescence", *J. Phys. Chem. C* **113** (28), 12095-12100 (2009), http://pubs.acs.org/doi/full/10.1021/jp9005668.
20. S. A. Maier, *'Plasmonics: Fundamentals and Applications'*, Springer, 2007.
21. M. Fan, G. F. S. Andrade, and A. G. Brolo, "A review on the fabrication of substrates for surface enhanced Raman spectroscopy and their applications in analytical chemistry",
Anal. Chimica Acta **693** (1-2), 7-25 (2011), http://dx.doi.org/10.1016/j.aca.2011.03.002.
22. G. A. Baker, and D. S. Moore, "Progress in plasmonic engineering of surface-enhanced Raman-scattering substrates toward ultra-trace analysis", *Anal. Bioanal. Chem.* **382** (8), 1751-1770 (2005), http://www.springerlink.com/content/h5523g21282h4733/.
23. Y. –J. Hung, I. I. Smolyaninov, C. C. Davis, and H. –C. Wu, "Fluorescence enhancement by surface gratings", *Opt. Exp.* **14** (22), 10825-10830 (2006), http://dx.doi.org/10.1364/OE.14.010825.
24. M. T. Zin, K. Leong, N. –Y. Wong, H. Ma, M. Sarikaya, and A. K. –Y. Jen, "Surface-plasmon-enhanced fluorescence from periodic quantum dot arrays through distance control using biomolecular linkers", *Nanotechnol.* **20** (1), 015305 (2009), http://iopscience.iop.org/0957-4484/20/1/015305/.
25. A. Kinkhabwala, Z. Yu, S. Fan, Y. Avlasevich, K. Müllen, and W. E. Moerner, "Large single-molecule fluorescence enhancements produced by a bowtie nanoantenna", *Nat. Photon.* **3** (11), 654-657 (2009), http://www.nature.com/nphoton/journal/v3/n11/full/nphoton.2009.187.html.
26. P. J. Schuck, D. P. Fromm, A. Sundaramurthy, G. S. Kino, and W. E. Moerner, "Improving the Mismatch between Light and Nanoscale Objects with Gold Bowtie Nanoantennas",
Phys. Rev. Lett. **94** (1), 017402 (2005), http://link.aps.org/doi/10.1103/PhysRevLett.94.017402.

27. J. M. Gerton, L. A. Wade, G. A. Lessard, Z. Ma, and S. R. Quake, "Tip-Enhanced Fluorescence Microscopy at 10 Nanometer Resolution", *Phys. Rev. Lett.* **93** (18), 180801 (2004), http://link.aps.org/doi/10.1103/PhysRevLett.93.180801.
28. F. M. Huang, F. Festy, and D. Richards, "Tip-enhanced fluorescence imaging of quantum dots", *Appl. Phys. Lett.* **87** (18), 183101 (2005), http://dx.doi.org/10.1063/1.2115073.
29. N. I. Cade, F. Culfaz, L. Eligal, T. Ritman-Meer, F. –M. Huang, F. Festy, and D. Richards, "Plasmonic Enhancement of Fluorescence and Raman Scattering by Metal Nanotips",
Nanobiotechnol. **3** (3-4), 203-2011 (2007), http://www.springerlink.com/content/t707k8x6845759k5/.
30. P. Mandal, and S. A. Ramakrishna, "Dependence of surface enhanced Raman scattering on the plasmonic template periodicity", *Opt. Lett.* **36** (18), 3705-3707 (2011), http://dx.doi.org/10.1364/OL.36.003705.
31. R. F. Kubin, and A. N. Fletcher, "Fluorescence quantum yields of some rhodamine dyes",
J. Lumin. **27** (4), 455-462 (1982), http://dx.doi.org/10.1016/0022-2313(82)90045-X.
32. E. J. Zeman and G. C. Schatz, "An accurate electromagnetic theory study of surface enhancement factors for silver, gold, copper, lithium, sodium, aluminum, gallium, indium, zinc, and cadmium", *J. Phys. Chem.* **91** (3), 634-643 (1987), http://pubs.acs.org/doi/abs/10.1021/j100287a028.
33. http://www.microresist.de/products/room_haas/pdf/ as on 29/6/2012.
34. J. M. Montgomery, A. Imre, U. Welp, V. V. –Vlasko, and S. K. Gray, "SERS enhancements via periodic arrays of gold nanoparticles on silver film structures", *Opt. Exp.* **17**(10), 8669-8675 (2009), http://dx.doi.org/10.1364/OE.17.008669.